Draft version March 6, 2017
Typeset using LaTeX **manuscript** style in AASTeX61

Herschel ORION PROTOSTAR SURVEY (HOPS) IMAGING AND PHOTOMETRY RESULTS.

Babar Ali,[1] William J. Fischer,[2,*] S. Thomas Megeath,[3] Elise Furlan,[4] Amelia M. Stutz,[5] Thomas Stanke,[6] John J. Tobin,[7] James Di Francesco,[8] Lori E. Allen,[9] Dan M. Watson,[10] T. L. Wilson,[11] and Thomas Henning[5]

[1]*Space Sciences Institute, Boulder, CO*
[2]*NASA Goddard Space Flight Center, Greenbelt, MD, USA.*
[3]*Ritter Astrophysical Observatory, Department of Physics and Astronomy, University of Toledo, Toledo, OH, USA*
[4]*Infrared Processing and Analysis Center, California Institute of Technology, 770 S. Wilson Ave., Pasadena, CA 91125, USA*
[5]*Max Planck Institute for Astronomy, Königstuhl 17, D-69117 Heidelberg, Germany*
[6]*European Southern Observatory, Garching bei Munchen, Germany*
[7]*Hubble Fellow, National Radio Astronomy Observatory, Charlottesville, VA 22903*
[8]*Senior Research Officer, National Research Council Canada, Vancouver, Canada*
[9]*National Optical Astronomy Observatory, Tucson, AZ, USA*
[10]*Department of Physics and Astronomy, University of Rochester, Rochester, NY, USA*
[11]*Naval Research Laboratory, Washington, DC, USA*

(Received; Revised March 6, 2017; Accepted)

Submitted to ApJ

ABSTRACT

We summarize and investigate observed far-infrared properties of 409 protostar candidates in the Orion A and B clouds using data from the *Herschel* Space Observatory. The observations were taken as part of the Open Time Key Program *HOPS* (*Herschel* Orion Protostar Survey, PI: S. T. Megeath). We find spatial correlations in the observed flux ratios as a function of sub-regions in both the Orion A and B clouds. Using simulations, we rule out completeness bias as the sole cause for the observed correlations. We offer differences in accretion properties and/or evolutionary status as,

Corresponding author: Babar Ali
bali67@gmail.com

at least partially, responsible for the observed differences by sub-regions. Both accretion properties and evolutionary status differences, in turn, may trace fundamental differences in the star-forming conditions in the respective environments.

Keywords: stars: protostars — stars: formation — infrared: stars — submillimeter: stars

* NASA Postdoctoral Program Fellow.

1. INTRODUCTION

A comprehensive theory of the formation of stars, which explains the origins of stars from the local raw materials and environmental conditions, is necessary for understanding processes spanning the entire range of cosmic evolution from the formation and evolution of galaxies to the formation of planets (Kennicutt & Evans 2012). Thus, a primary goal of current Galactic star-formation research is to develop such a comprehensive theory of star formation. However, many details and key ingredients needed to complete our picture of the star-formation process are not well understood (McKee & Ostriker 2007). In particular, one critical aspect, the connection between the raw materials and the final product (the star) is not well characterized (Dunham *et al.* 2014). In other words, while the building blocks and the conditions for the formation of stars are provided by the underlying environment the influence of said environmental conditions on the subsequent population is not understood. The importance of star-formation is underscored by the expansive open and guaranteed-time legacy-class observing programs scheduled on major space-based observatories *Spitzer* (Werner *et al.* 2004), and *Herschel* [1] (Pilbratt *et al.* 2010).

Protostars provide useful laboratories for studying said connection between the local environmental conditions and the star itself. At the protostellar stage, the incipient star is still strongly connected with the local environment, and it is in the protostellar phase that the stellar mass is accumulated and protoplanetary disks are created (Evans *et al.* 2009). A detailed characterization of the protostellar evolution, thus, allows us to directly follow the evolution of raw materials into a star. Yet, despite its fundamental importance, there is no generally accepted theory describing the evolution of a protostar from the initial stages when it is deeply embedded in a cloud core to the late stages when it is transitioning to a pre-main sequence star+disk system (Dunham *et al.* 2014).

Two items, in particular, make studying protostars difficult: (i) observational studies must be able to disentangle the degenerate effects of both the environment and the star-formation process itself. (ii) The presence of dust in the local environment means the amount of extinction in lines-of-sight to

[1] In fact, the former name of *Herschel*, FIRST was an homage to one of primary objectives of *Herschel*: the study of the first stars and galaxies in their earliest stages.

star formation regions is abnormally high (few to several tens of magnitudes in the visual) compared to most of the rest of the Galaxy. To tackle (i), we chose to study a large number of protostars in the Orion molecular cloud complex. Orion provides several key advantages for such studies. Megeath *et al.* (2012) identified a rich sample of protostars in Orion from *Spitzer*. At 419 pc, Orion is relatively nearby (Schlafly *et al.* 2014) and, thus, allows excellent spatial resolution. Star formation has been observed in a rich diversity of environments, from isolated cold globules to rich clusters. See, for example, Carpenter (2000), Feigelsen *et al.* (2005), Stutz *et al.* (2010).

Spitzer and *Herschel* observations, in particular, confirmed long recognized views that far-IR observations of the reprocessed radiation can probe the evolution of protostars (Adams, Lada, & Shu 1987). The presence of an infalling envelope of gas and dust is the defining characteristic of a protostar. This envelope absorbs the radiation from the central accreting star+disk and reprocesses most of the luminosity into the far-IR (Ali *et al.* 2010). Far-IR observations are, therefore, absolutely crucial for efficiently identifying and studying protostars because protostars emit most of their light in those wavelengths.

This paper summarizes the results from the photometry component of the *Herschel* Orion Protostar Survey (HOPS) Open Time Key Program (PI: S. T. Megeath). This paper is one in a series describing the results from HOPS (*e.g.* Stutz *et al.* 2013, Kryukova *et al.* 2014, Fischer *et al.* 2016, Furlan *et al.* 2016). Our emphasis in this paper will be on the photometry catalog and the observed properties of protostars. Section 2 describes our observational sample and technique. Section 3 describes our data processing and assembly of final maps. Section 4 discusses photometry of individual sources. Sections 5 & 6 present and discuss our findings. And, finally, our conclusions are summarized in Section 7.

2. PROTOSTAR SAMPLE & OBSERVATIONS

The *Spitzer* Orion protostar sample was defined and described by Megeath *et al.* (2012). We selected a flux-limited subset of 280 protostars for follow-up with *Herschel* for HOPS. The number of targets for HOPS follow-up was limited solely by signal-to-noise ratio (S/N) considerations. All 280 *Herschel* targets were segregated in distinct spatial tiles to optimize observing. The tiles were assigned consecutive three-digit integer group numbers starting with the number 0 (zero). The spatial sizes of the tiles ranged from 3′ (most common) to 7′ (CAN SOMEONE WITH ACCESS TO RAW DATA CONFIRM THE LARGEST FOV?). The protostar candidates selected for our *Herschel* survey are referred to as the HOPS sources and are uniquely identified by a 3-digit integer number starting with the number 0 (zero). Ultimately, we detected additional candidates previously identified in the *Spitzer* survey whose spatial location happened to be within the field-of-view of the observation tile. These sources, however, were not part of the original HOPS candidate list because their estimated fluxes were below our S/N limit. Further, Stutz *et al.* (2013) found protostars and candidates not identified in the *Spitzer* list; See section 2.2 for more details. Our final catalog appends the original sample of 280 targets with the additions mentioned above. There are a total of 409 sources in the final sample included here. Note that Furlan *et al.* (2016) also include one additional source from Tobin *et al.* (2015) which was not available when the analysis for this work was completed.

Furlan *et al.* (2016) classified 330 of these sources as young stellar objects (YSOs) and the remaining as unlikely to be protostars and/or sources not observed or detected by PACS at 70 micron. For their analysis, Furlan *et al.* (2016) focus on the 330 HOPS targets which have complete *Spitzer* and *Herschel* data (at least a PACS 70 μm detection) and most were originally considered protostars by Megeath *et al.* (2012). The objective of this contribution is to provide complete data on all sources from our original sample of 280 protostars as well as the additional targets detected in our images. Thus, we have included all 409 objects in this contribution.

2.1. *Observing strategy*

For the HOPS Key Program, we used the PACS instrument (Poglitsch *et al.* 2010), and the scan-map Astronomical Observing Template (AOT) with the 20″/second scan speed. The scan map AOT offers several advantages over the point source, small source, and raster AOTs: (i) scan-map AOTs ultimately provide the best sky sampling. (ii) Scanning allows efficient mapping of groups of point-sources within individual spatial tiles. And, (iii) PACS' non-scan AOTs must employ chopping to remove background and low- frequency drifts; Chopping cannot provide optimal removal of these effects in spatially confused regions such as the protostellar fields in Orion.

We used the slowest allowed scan speed (20″/second) to avoid beam smearing and to preserve the best possible spatial resolution. By design, the PACS instrument observed both the 70 μm and 160 μm filters simultaneously. Each group of stars (spatial tile) was observed in two scan directions to avoid the so-called *striping* defect common to bolometer arrays (Tegmark 1997). These two scan directions form two distinct *Herschel* Astronomical Observing Requests (AORs). Hence, each group in our observations is assigned two separate unique identifiers, called OBSIDs. The two AORs per group are concatenated and were, therefore, assigned sequential OBSIDs. Typically, several scans are needed to cover our spatial tiles given that the size of the spatial tiles (see above) is larger than the PACS field-of-view. We allowed the PACS observing template to automatically calculate the number of scans and overlap between each scan for our required sensitivity and tile size. Our observing template observed the spatial tile with uniform coverage.

2.2. *The observed protostar sample*

Table 2 lists the final combined catalog (see below for Table details). As noted above, in some groups, we coincidently observed additional protostars from the Megeath *et al.* (2012) *Spitzer* sample. These sources happen to be located inside group fields-of-view. Of note, Stutz *et al.* (2013) identified highly embedded additional protostars (the so-called PACS Bright Red Sources, PBRs). Our final catalog includes all known protostars detected by *Herschel* in the Orion fields covered by our observations.

We investigated HOPS images for additional protostar candidates that might have been missed by our earlier efforts. Stutz *et al.* (2013) required a 160 μm detection for improved reliability, and implemented additional thresholds to reduce contamination from extra-galactic sources. As Stutz *et al.* (2013) showed, *Spitzer* observations did not identify, or in rare cases, detect all protostars in Orion. Hence, the possibility remains that additional sources, perhaps with detections only in the 70 μm filter, lurk within our data. With detection in only one or two bands, however, it is increasingly difficult to properly characterize these sources and distinguish them from foreground or background objects. It is likely necessary that additional protostar candidates here will require follow-up observations or analysis. Nonetheless, these sources may impact statistical studies, and are tabulated. The results of this effort will be described in a future contribution.

The columns have the following meaning in Table 2. Column 1 lists the unique three-digit HOPS identifier. Columns 2 & 3 list the J2000 equatorial coordinates as measured on the *Herschel* images and as reported by the DAOPHOT find algorithm (Stetson 1987). Column 4 lists the *Herschel*-assigned unique observation identifiers (OBSIDs, two per group as described in Section 2.1). Column 5 lists the 3-digit group number mentioned above. Columns 6-11 list the *Herschel* photometry for the three Herschel/PACS bands. Our photometry procedure is described in Section 4. The 70 μm and 160 μm flux densities are from our program. The 100 μm fluxes are added from the larger survey of the Orion region from the the Gould-Belt Key Program (Konyves *et al.* 2010). The extraction of the 100μm photometry is discussed in Stutz *et al.* (2013). Each photometry value is described by two columns: the first provides the photometry value itself, and the other, labelled flag, has the following meaning: flag = 0 means the source is not observed. flag =1 means the photometry, as quoted, is the measured value, flag = 2 means the value is an upper limit, and flag = 3 means that the measurement is from the PSF-photometry, not aperture photometry (see Section 4). Column 12 identifies the sub-region within the Orion A and B clouds to which the HOPS source belongs. The sub-region definitions are listed in Table 1. Finally, Column 13 lists the UT observation day for the observations. When a source was detected in more than one group (tile) we combined the measurements as a simple average.

3. DATA PROCESSING & MAP-MAKING

We start data processing at the level 1 stage from the Herschel Science Archive. Level 1 contains calibrated timelines[2] from individual PACS bolometers from which all instrumental effects have already been removed except for the low frequency noise component (the so-called 1/f noise[3]). Our processing mitigates the 1/f noise, combines the two independent orthogonal scan directions, and

[2] Timelines are simply readouts from individual pixels ordered sequentially by time of observation. Note that for our observations the PACS instrument was used with a fixed readout frequency of 10 Hz.

[3] The so-called 1/f noise modifies the signal timelines by adding a drift component whose amplitude is a power-law function of its Fourier frequency.

projects the timelines onto the final image of the field. We will refer to these steps as 'map-making' hereafter. The processing steps leading up to level 1 are described in Poglitsch *et al.* (2010) and in the data processing guides for the Herschel Interactive Processing System, HIPE Ott *et al.* (2010). All data discussed here are based on the FM7 version of the PACS calibration (Balog *et al.* 2013) and processed with version 9 of the HIPE software. Our final maps have spatial scales of 1.6″/pixel and 3.2″/pixel for the 70 μm and 160 μm PACS filters, respectively. We used three different approaches for map-making that are described below.

3.1. *The High Pass Filter (HPF) branch*

This technique filters bolometer timelines and, as the name suggests, blocks all temporal frequencies lower than the filter width (conversely, it allows only temporal frequencies smaller than the filter width). Such filtering removes the low-frequency signal present in the timelines from both the 1/f noise as well as from astrophysical sources. The primary advantage is that point sources, whose temporal frequencies are higher than the chosen filter width, are preserved. Thus, this branch is useful for point source photometry. The HPF filtering was applied as follows: First, for any given readout in the timeline, the median value is calculated within a window of preceding and following readouts. Only those readouts that are not flagged as a glitch or otherwise identified as problematic are included in the calculation. Second, this median value is subtracted from the signal value in the current readout. The process is repeated for all readouts in the timeline. We investigated several different HPF filter window widths and settled on 15 readouts (1.5 seconds) and 20 readouts (2 seconds) for the 70 μm and 160 μm filters, respectively. These provided the optimal balance between preserving the signal from point sources and filtering out as much of the 1/f noise as possible. We use the HPF branch as implemented in HIPE and described by Popesso *et al.* (2012).

For the HPF filtering, we assume that the median value determines the local sky emission and any variations in this median value are purely due to the drift caused by 1/f noise. However, there is substantial amount of spatially extended emission in our fields from the molecular cloud itself (this emission is also referred to as nebulosity). This widespread emission has the undesired effect of altering the median values. Thus, along with the 1/f noise, the extended spatial emission (nebulosity) is also removed by the HPF processing because the value of the local sky (taken as the median, see above) includes emission from local nebulosity. In addition, point sources themselves may also elevate the median value in the HPF filter. Thus, we mask and exclude point sources from the median calculation. These masks are generated from the first iteration of HPF map-making and used in the 2nd iteration. We use maps only from the 2nd iteration for our analysis. We investigate the effect of nebulosity on the HPF and its consequences on the subsequent photometry in Section 4

3.2. *The Scanamorphos branch*

Scanamorphos is a map-making software developed and described by Roussel (2012). Scanamorphos removes the low-frequency noise by making use of the redundancy built in the observations. Readers are referred to Roussel (2012) for details about the processing steps. Stutz *et al.* (2013) also used Scanamorphos-created maps for their Orion study. Unlike the HPF branch Scanamorphos preserves astrophysical emission on all spatial scales, ranging from point sources to extended structures with scales just below the map size. Scanamorphos maps are, thus, suitable for both spatially extended and point sources.

3.3. *MADmap branch*

We compared our Scanamorphos reduced images with those produced by another map-making option available within HIPE: the MADmap branch based on a java implementation of the Maximum Anisotropy Dataset mapper (MADmap) software developed and described by Cantalupo *et al.* (2010). As with Scanamorphos, MADmap images preserve fluxes on all spatial scales in the field-of-view. At the time these data reductions were applied, the MADmap branch suffered from the so-called point-source-artifacts (Piazzo *et al.* 2012); Hence, the primary use of MADmap was in allowing us to check our Scanamorphos images for any spurious artifacts introduced by the map-making process. We looked for structures that were present in one, but not both images from the two map-making approaches. Such artifacts may result from the map-making process in fields such as Orion because the Fourier frequencies of extended, nebulous emission are similar in nature to the low-frequency drift (the 1/f noise). Thus, it becomes necessary to verify that the process by which 1/f noise is removed does not affect or alter flux from spatially extended sources. The MADmap branch provided said quality control for our fields.

4. PHOTOMETRY

Photometry is notoriously difficult in star-forming regions in particular. Specific challenges are: (i) differentiating spatially unresolved knots in the nebular emission from actual point sources, (ii) estimating the local background contribution. The nebular emission is usually complex and contains gradients of emission at all spatial scales that violate background homogeneity assumptions commonly used in aperture photometry and Point Spread Function (PSF)-fitted photometry algorithms. (iii) Disentangling close binaries. Further, protostars have a higher binary frequency than their main-sequence counterparts (Reipurth *et al.* 2014). We, therefore, rely on multiple approaches in both map-making and photometry to resolve these issues. The final list of photometry values is determined by combining the multiple approaches by considering the relative merits (strengths and weaknesses) of each approach for each source individually.

4.1. *Aperture photometry*

Stutz *et al.* (2013) and Furlan *et al.* (2016) describe the details of the aperture photometry procedure we followed for our images. For convenience, we briefly reprise the salient points here: We used the HPF branch images for aperture photometry measurements. To avoid nebular contamination from the local environment, we place the inner annulus of our apertures as spatially close to the source as possible. This step necessitates customized aperture corrections since the background annuli include a significant fraction of a source's point spread function (PSF) profile. We used the Vesta calibration image (PACS's PSF standard, see Lutz *et al.* 2012) to calculate aperture corrections. We set the inner radius of sky annulus to the aperture radius to ensure the sky annulus sample the spatially varying nebulosity near the source. The adopted values for 70 μm are 9.6$''$, and 19.2$''$, for the aperture and sky annuli, respectively. The aperture correction factor is 0.7331. In the 160 μm images, the adopted values are 12.8$''$, and 25.6$''$, for the aperture and sky annuli, respectively. The aperture correction factor at 160 μm is 0.6602.

The aperture photometry technique has several factors in its favor: First, it is a reliable and well-understood technique. Next, it is the technique used for flux calibration of the PACS instrument (Balog *et al.* 2013). Further, the use of narrow apertures as described above alleviates nebular contamination and source crowding issues for most sources. However, the complex structure in the images means that brightnesses for a significant fraction of sources are not well measured using aperture photometry. The primary issue is the presence of a source or strong nebular emission in either the aperture or the sky annulus. The sky annulus can be particularly affected by the presence of a strong source given that we have opted to use fairly narrow sizes for them (hence, small number of pixels are available for sky estimation). These issues affect the 160 μm image more strongly because there is simply more emission detected at that wavelength. For these subset of sources, it was necessary to use a secondary photometry technique that is less susceptible to the issues noted above. The next two subsections describe our method for identifying contaminated aperture photometry sources.

4.2. *Point Spread Function (PSF) fitted photometry*

The PSF photometry technique fits a known spatial profile for point sources to the measured point source profiles, and determines their brightnesses by the amount of scaling needed between the known and measured profiles (Stetson 1987). This scaling (hereafter referred to as the PSF amplitude) is the main quantitative measurement in this technique. The primary advantage is that the PSF-fitting technique disentangles the spatial profile of the source from other point sources and nebular contamination. Thus, it is less affected by the issues noted for aperture photometry above. This technique, however, requires that the source PSF profiles are well-characterized. Given that no clean (contamination-free) sources are available in our HOPS fields, we used the Vesta images (Lutz 2012) as proxy for the PSF profiles for our sources. We note that PACS's PSF is highly non-axisymmetric (Lutz 2012). To remove any systematical photometry offsets between PSF-based photometry and aperture-based photometry, we repeated the PSF measurements on a subset of PACS' flux standard stars. This comparison allowed us to calibrate measured PSF amplitudes and actual flux values, as described below.

We used the *Starfinder* package (Diolaiti *et al.* 2000) for fitting PSF profiles and measuring photometry values of sources in the Scanamorphos-reduced images. The *Starfinder* source finding algorithm suffers from the same challenges as other source-finding algorithm in that many of the detected sources are unresolved compact structures in the nebular emission. We, therefore, limit our PSF-fitted photometry only to known protostars with aperture photometry issues as noted above. The remaining sources are ignored.

As mentioned earlier, the *Starfinder* PSF amplitudes must be adjusted to remove any systematic bias in PSF photometry. To that end, we processed PACS observations of flux standard stars taken in the same manner as our program stars. Then, we used *Starfinder* on these fields using exactly the same parameter set used for the HOPS program images. The measured PSF amplitudes for the flux standards and knowledge about their actual fluxes provides the necessary calibration between the two.

4.3. *Final photometry selection*

We inspected each HOPS protostar image individually. First, visual inspection was used to identify contaminants: *e.g.* other point sources within the aperture radius, or strong nebular features that are likely to affect photometry. Once identified as problematic, we considered both PSF-fitted and aperture photometry in the context of the overall spectral energy distribution (SED) for the source. Aperture photometry for sources with strong contaminants is rejected in favor of PSF-fitted photometry.

4.4. *100 μm photometry*

The 100 μm photometry listed in Table 2 is taken from the *Herschel* Gould Belt Survey Key Program (PI: Phillippe Andre). Stutz *et al.* (2013) describes our motivation for including the 100 μm photometry, as well the details about the photometry procedures. For the 100 μm photometry, we relied only on aperture photometry values.

5. RESULTS

Table 1. The sub-region boundaries in the Orion A & B clouds

Name	Declination Boundary (degrees)		Number of protostars
	Low	High	
LDN 1622	1.3	2.0833	11
NGC 2068	-0.5	1.3	59
NGC 2023/4	-3.83	-0.5	27
OMC 2/3	-5.30	-3.83	64
ONC-S	-6.10	-5.30	54
LDN 1641-N	-6.90	-6.10	47
LDN 1641-C	-7.60	-6.90	62
LDN 1641-S	-9.0	-7.60 85	

In this contribution, we focus on the *observed* properties of the target protostars. A series of companion publications, Fischer *et al.* (2016), Furlan *et al.* (2016), Kryukova *et al.* (2014), and Stutz *et al.* (2013) present results and analysis from other scientific investigations and interpretations using these data from the HOPS program. We further restrict our attention to the observed differences between the sub-regions of both Orion A and B clouds. In particular, we have elected to examine the following relationships: (i) flux distributions, (ii) color distributions, and, (iii) slopes of the SEDs. We augment our analysis with previously published results for the PBR sources Stutz *et al.* (2013), and sub-mm photometry (Stanke *et al.* 2015). We present results from each of the above identified observation quantity below, and collectively discuss the picture of star-formation implied by these observations in Section 6.

5.1. *Flux distribution functions*

Figure 1 shows the flux distribution (FD) functions at 70 μm and 160 μm, respectively, for all 409 sources detected in our sample. Figures 2 & 3 show the flux distributions segregated by sub-region, and separately for the Orion A (left column) and Orion B (right column) clouds. The sub-region and the number of associated sources are identified within the sub-panels of the Figures. We do not consider upper limits in these FDs (sources with flag value = 2 in Table 2). There are distinct differences apparent in the observed flux distributions as a function of sub-region. We note that in a flux-limited survey, such as ours, local environmental differences in the amount and structure of the nebular emission can significantly bias source detection and photometry algorithms. We quantify FD differences and investigate the role of bias below.

The 70 μm FDs are relatively flat (*i.e.*, the number of sources in all bins is similar) for the Orion B sub-regions: LDN 1622, NGC 2068, and NGC 2023/4. This situation is likely due to the low numbers of protostars available for each sub-region. In Orion A, the 70 μm FDs have an apparent peak at or near 1 Jy in all sub-regions. And, no significant differences are obvious between sub-regions, except for LDN 1641-N.

The 160 μm FDs show clear and obvious differences amongst the sub-regions. The following results, in particular, are noted: (i) there is a complete lack of sources below $\sim$500 mJy in OMC-2/3 region. (ii) The LDN 1641 (all) and OMC 2/3 sub-regions have apparent peaks in FDs at different flux values. (iii) The peak of the ONC-S flux distribution is between those of LDN 1641 and OMC 2/3. And, (iv) in Orion B, LDN 1622 and NGC 2023/4 show differences in the observed distribution, even with the low number of sources available.

The 160 μm FDs suggest a trend of increasingly bright sources towards lower declinations in Orion B, and increasingly bright sources towards higher declinations in Orion A. We investigate this apparent trend by plotting the median flux for each sub region as a function of declination. Figure 4 shows the resulting quantitative correlations. The median shows a systematic change as a function of declination (sub-region) as noted above. The trend is, however, weakly noted in the 70 μm fluxes, and shows OMC 2/3 region with significantly different median flux for the 160 μm fluxes. The implications for this result are discussed in Section 6.

5.2. *Flux ratio distribution*

Flux ratios (colors) are better suited for determining differences as a function of source type than the flux itself because flux ratios depend on the shape of the source SED (Ali *et al.* 2010). We investigated two different flux ratios using the combined Spitzer, HOPS and Gould-Belt photometry: $\mathrm{Log}_{10}(\lambda F_\lambda 70/\lambda F_\lambda 24)$, and $\mathrm{Log}_{10}(\lambda F_\lambda 160/\lambda F_\lambda 100)$. Figures 5 & 6 show the flux-ratio vs flux-ratio plots segregated by sub-region for Orion A and Orion B. We do not include data with upper limits for these plots (sources with flag value = 2 in Table 2). The red symbols show the colors for the sub-region identified in the sub-panel, and the black symbols show the colors for the entire sample. As with the median of the FD, we note an apparent systematic change in the observed flux ratios relative to the entire population in both Orion A and Orion B.

We quantitatively explore this apparent trend further in Figures 7 & 8. These Figures show the mean and median colors for each of the sub-regions as a function of the mean declination for all sources belonging to the respective sub-region. Since the sub-regions are vertically segregated in both the Orion A and B clouds, declination is a useful proxy for sub-region.

In Orion A, the median and mean colors of the sub-regions become systematically redder towards higher declinations. In Orion B, the median and mean colors of the sub-regions becomes systematically redder towards lower declinations. For both, the vertical bar shows the 1-σ standard deviation of the flux-ratio values as a proxy for the range. Even with large variation in color, the systematic trends with declination is clearly delineated.

5.3. *Number of protostars*

Table 1 and Figure 9 list and show the numbers of HOPS protostars as a function of sub-region within the Orion A and Orion B clouds. Since the proto-stellar phase lasts <1 Myr (Megeath *et al.* 2012), the observed number of protostars may trace the sites where high rates of recent star-formation are transpiring. We note, however, that Stutz *et al.* (2013) find that Orion B, which has the fewest protostars, have the most PBRs, suggesting youth.

6. DISCUSSION

The results presented in Section 5 show the global properties of the HOPS protostar sample. Since the sub-regions in Orion A and B are well stratified by declination, differences are easily explored by using declination as a proxy for sub-region. Indeed, Figures 4, 7, & 8 show that systematic variations exist in the observed proto-stellar properties as a function of declination in the Orion A & B clouds. We discuss in Sections 6.1 & 6.2 two explanations of this observed trend. Again, we will restrict ourselves to observed quantities only and leave the detailed exploration of inferred properties to companion papers.

6.1. *Completeness limit bias*

Completeness limits are difficult to estimate accurately. The detection efficiency is a strong function of the magnitude of the local nebular emission; Hence, we expect the limits to vary considerably even within a single sub-region as the nebular emission itself varies inside any of our adopted sub-region boundaries. This variation makes it difficult to disentangle observational bias from any real trends shown in Figures 4, 5, & 6.

Fortunately, there is a way to decouple detection bias. Differences in completeness limit will affect the median flux distribution (Figure 4), since such differences will bias the median calculation. For the same effect to exist also in the flux ratio correlation (Figures 5 & 6) requires that the observed flux be correlated with flux ratio. We investigate this possibility by directly examining the data for such a correlation, and via a simple simulation described below.

Figure 10 shows the observed 70 μm flux as a function of the flux ratios used in our investigation. We note a marginal dependence of 70 μm flux with the $\mathrm{Log}_{10}(\lambda F_\lambda 70/\lambda F_\lambda 24)$ color, and no obvious correlation with $\mathrm{Log}_{10}(\lambda F_\lambda 160/\lambda F_\lambda 100)$. The first trend is not surprising because the protostar flux is dominated by the envelope whose SED peaks near 70 μm. Indeed, 70 μm flux changes likely track changes in the amount of material present in the envelope. In addition, material deeper inside the envelope (closer to the protostar) will be warmer and, hence, will emit more brightly at 70 μm than at 100 μm or 160 μm. Therefore, we expect to notice the equivalent of a hotter black body with lesser envelope material. The $\mathrm{Log}_{10}(\lambda F_\lambda 160/\lambda F_\lambda 100)$ color samples the Rayleigh-Jeans side of the SED peak and should show only marginal variation with changing temperature. On the other hand, the $\mathrm{Log}_{10}(\lambda F_\lambda 70/\lambda F_\lambda 24)$ color samples the Wien side of the SED and is more likely to show some variation. Following this reasoning, we understand the loose correlation seen only between 70 μm flux and $\mathrm{Log}_{10}(\lambda F_\lambda 70/\lambda F_\lambda 24)$ in Figure 10.

We can now further investigate completeness limit and observational bias via a simple simulation. The LDN 1641 sub-regions contain the largest number of protostars (see Table 1) and visual inspection shows the least contamination of the sample from extended nebulosity. Further, fainter protostars are detected in LDN 1641 than in Orion OMC 2/3. Hence, if bright, complex, spatially extended emission from the local dust is responsible for decreased reliability and higher completeness limits for point source photometry, then LDN 1641 provides an ideal contrast to the Orion OMC 2/3 sub-region. The contrast between LDN 1641 and Orion OMC-2/3 is at the extreme ends of the spatial correlation observed in Figures 4– 6.

We can simulate the bias introduced by completeness limit for OMC-2/3 by restricting the observed fluxes in LDN 1641 to only those protostars that are above a simulated completeness limit and recomputing statistical averages. We require that the population of protostars be fundamentally the same between OMC-2/3 and LDN 1641. If this assumption is not valid, then actual population differences must exist between the two sub-regions. (This scenario is discussed below in Section 6.2). We then re-calculate the mean color of LDN 1641 from the restricted sample. Figure 11 shows the result of our simulation on a plot of median flux ratio vs the completeness limit for LDN 1641 (solid line) and Orion OMC-2/3 region (dashed line). The top panel shows the results for median $\mathrm{Log}_{10}(\lambda F_\lambda 70/\lambda F_\lambda 24)$, and the bottom panel for median $\mathrm{Log}_{10}(\lambda F_\lambda 160/\lambda F_\lambda 100)$.

The median flux ratio, $\mathrm{Log}_{10}(\lambda F_\lambda 160/\lambda F_\lambda 100)$, in Figure 11 (bottom panel) remains nearly constant as the simulated completeness limit is increased. **We conclude that observational bias cannot explain the correlation seen in Figure 8**. On the other hand, observational bias does become significant for $\mathrm{Log}_{10}(\lambda F_\lambda 70/\lambda F_\lambda 24)$ when the completeness limit is near 0.5 Janskys. These conclusions support the results shown in Figure 10 that 70 μm flux is correlated with $\mathrm{Log}_{10}(\lambda F_\lambda 70/\lambda F_\lambda 24)$, but not with $\mathrm{Log}_{10}(\lambda F_\lambda 160/\lambda F_\lambda 100)$. Actual population differences between the sub-regions, however, cannot be ruled out. In the absence of completeness bias for $\mathrm{Log}_{10}(\lambda F_\lambda 160/\lambda F_\lambda 100)$, it is difficult to explain how the correlation in Figure 8 does not reflect actual differences in the underlying populations. $\text{Log}_{10}(\lambda F_\lambda 160/\lambda F_\lambda 100)$is insensitive to extinction and directly measures the reprocessed light from protostellar envelopes. We postulate that because actual population differences are impossible to rule out for $\text{Log}_{10}(\lambda F_\lambda 160/\lambda F_\lambda 100)$, then the changes in flux ratio with declination shown in Figure 7 must at least partially reflect real population differences between the sub-regions.

6.2. *Population differences*

We also consider the implications if the correlations shown in Figure 7 & 8 are due to systematic differences in the observed population as a function of sub-region. Ali *et al.* (2010) show that *Herschel* colors become redder with increasing envelope mass (envelope accretion rate). In fact, the envelope accretion rate is the dominating factor in setting colors. We rule out inclination as a factor because no reasonable justification can be made for systematic differences in inclination as a function of sub-region in Orion. Thus, we focus on differences in envelope properties. When interpreted as such, Figures 7 & 8 imply that either the accretion process is different amongst the sub-regions, or that the protostars are at systematically different stages of development in each sub-region. Both scenarios thereby conspire to lead to systematic differences in the envelope properties of the protostars.

If we surmise that the accretion process is the leading cause, then there are two means to achieve this end: (i) the available gas and dust contributing to the envelope is systematically different between the sub-regions, or (ii) the central cores are systematically more massive in regions with redder colors. Both scenarios may, in fact, point to simply having higher gas+dust densities and higher gas+dust content to explain redder colors. We conclude that the observed properties of *Herschel*-detected protostars in Orion are consistent with predicted differences in populations implied by differences in gas column densities and star-formation scenarios in the region.

Megeath et al (TOM, what reference goes here?) argue that regions with higher density may speed up protostellar evolution because collapse time-scales are dependent on the local density of material. Thus, the observed trends in Figures 7 & 8 may alternatively be viewed as differences in the evolutionary status of the protostars. To explain the trend, the protostars in the Orion OMC-2/3 and ONC sub-regions are required to have transferred more of their mass in the central cores, which leads to more accretion and higher infall rates. While similar to differences in the accretion processes, this scenarios suggests a fundamental difference in the star-formation process itself between sub-regions.

7. CONCLUSIONS

We explored the mid- to far-infrared properties of the Orion protostars obtained as part of the *Herschel*Key Program HOPS. Investigations of the observed properties of these protostars reveal apparent correlations as a function of sub-regions in both the Orion A and B clouds. We investigated the role of bias introduced due to differences in completeness limits in these correlations by artificially introducing a completeness limit in the LDN 1641 sub-region and comparing the resulting changes in median flux ratio to Orion OMC-2/3 values. These simulations suggest that completeness limit bias alone is not sufficient to explain the observed correlation for $\mathrm{Log}_{10}(\lambda F_\lambda 160/\lambda F_\lambda 100)$. An alternative explanation may be population differences between these sub-regions. We offer differences in accretion properties and/or evolutionary status as the cause for the population differences. We note that both accretion properties and evolutionary status trace fundamental differences in the star-forming conditions in the environment, notably higher gas+dust content. This contribution focused entirely on the observed photometry and flux ratios. Companion publications will explore the environmental differences by examining derived quantities such as bolometric properties and classification.

BA was partially supported with NASA grant IPAC.ALI-OTKP-1-JPL.000094 for this work. The work of W. F. was supported in part by an appointment to the NASA Postdoctoral Program at Goddard Space Flight Center, administered by Oak Ridge Associated Universities through a contract with NASA.

The work of AMS was partially supported by the Deutsche Forschungsgemeinschaft priority program 1573 ("Physics of the Interstellar Medium").

J. Tobin acknowledges support provided by NASA through Hubble Fellowship grant HST-HF-51300.01-A awarded by the Space Telescope Science Institute, which is operated by the Association of Universities for Research in Astronomy, Inc., for NASA, under contract NAS 5-26555. The National Radio Astronomy Observatory is a facility of the National Science Foundation operated under cooperative agreement by Associated Universities, Inc.

The Herschel spacecraft was designed, built, tested, and launched under a contract to ESA managed by the Herschel/Planck Project team by an industrial consortium under the overall responsibility of the prime contractor Thales Alenia Space (Cannes), and including Astrium (Friedrichshafen) responsible for the payload module and for system testing at spacecraft level, Thales Alenia Space (Turin) responsible for the service module, and Astrium (Toulouse) responsible for the telescope, with in excess of a hundred subcontractors.

PACS has been developed by a consortium of institutes led by MPE (Germany) and including UVIE (Austria); KU Leuven, CSL, IMEC (Belgium); CEA, LAM (France); MPIA (Germany); INAF-IFSI/OAA/OAP/OAT, LENS, SISSA (Italy); IAC (Spain). This development has been supported by the funding agencies BMVIT (Austria), ESA-PRODEX (Belgium), CEA/CNES (France), DLR (Germany), ASI/INAF (Italy), and CICYT/MCYT (Spain).

HIPE is a joint development by the Herschel Science Ground Segment Consortium, consisting of ESA, the NASA Herschel Science Center, and the HIFI, PACS and SPIRE consortia.

Facilities:

Facility: Herschel Space Observatory (PACS)

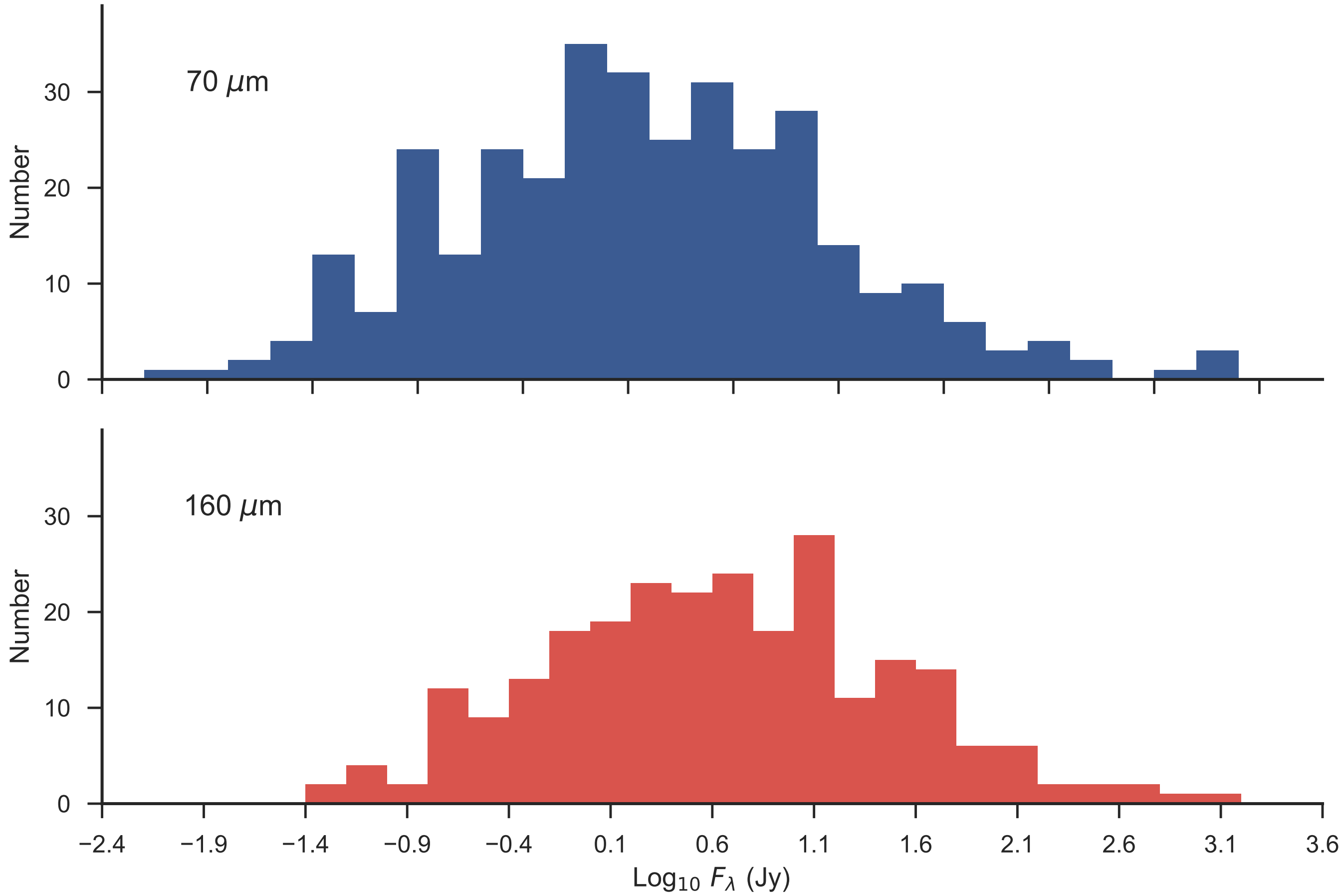

Figure 1. Flux distributions at 70 μm (top, blue) and 160 μm (bottom, red) for all sources in the HOPS sample. The upper limits are not used to calculate the distribution.

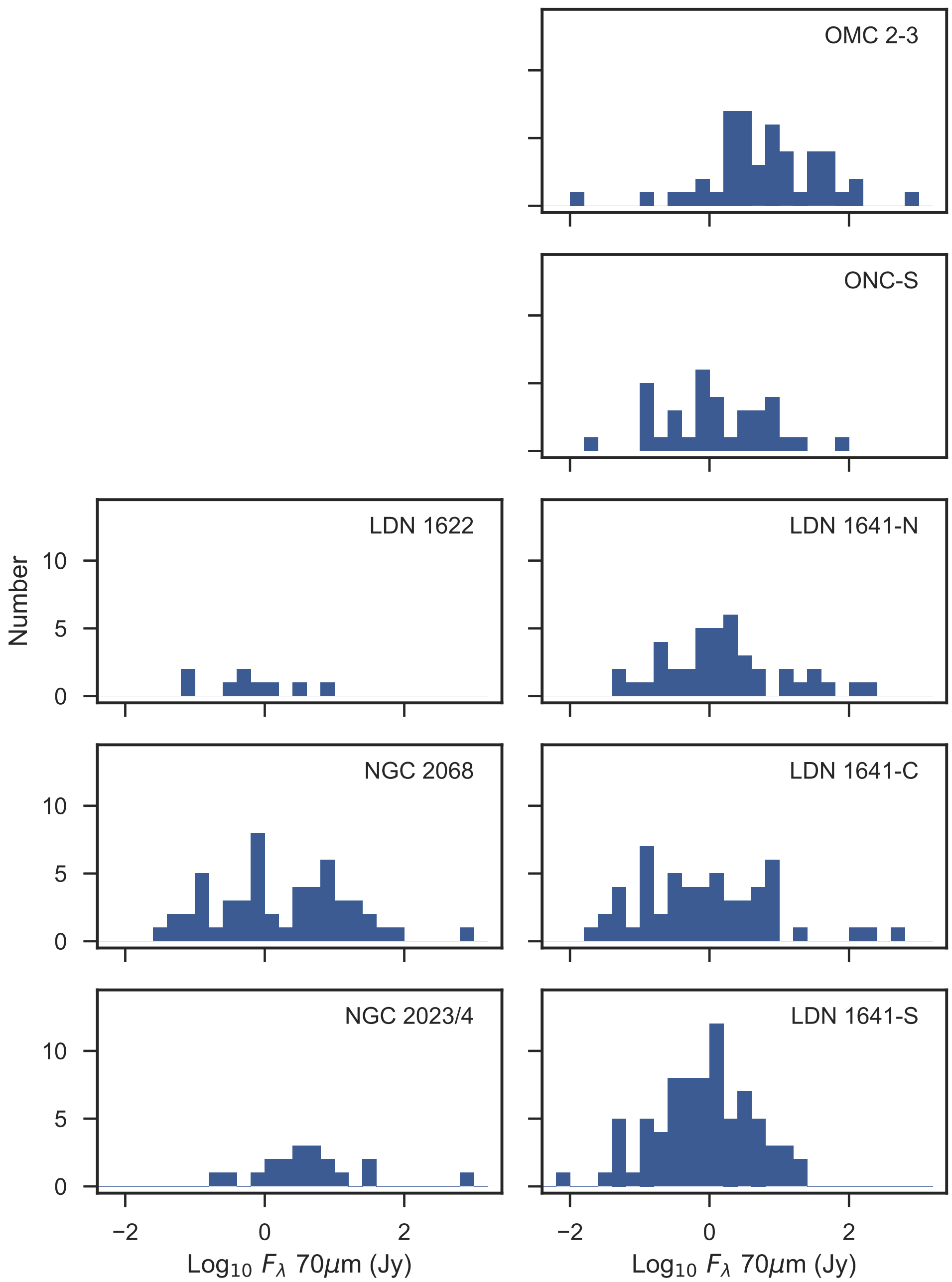

Figure 2. The 70μm flux distributions segregated by sub-region for Orion B (left column) and Orion A (right column).

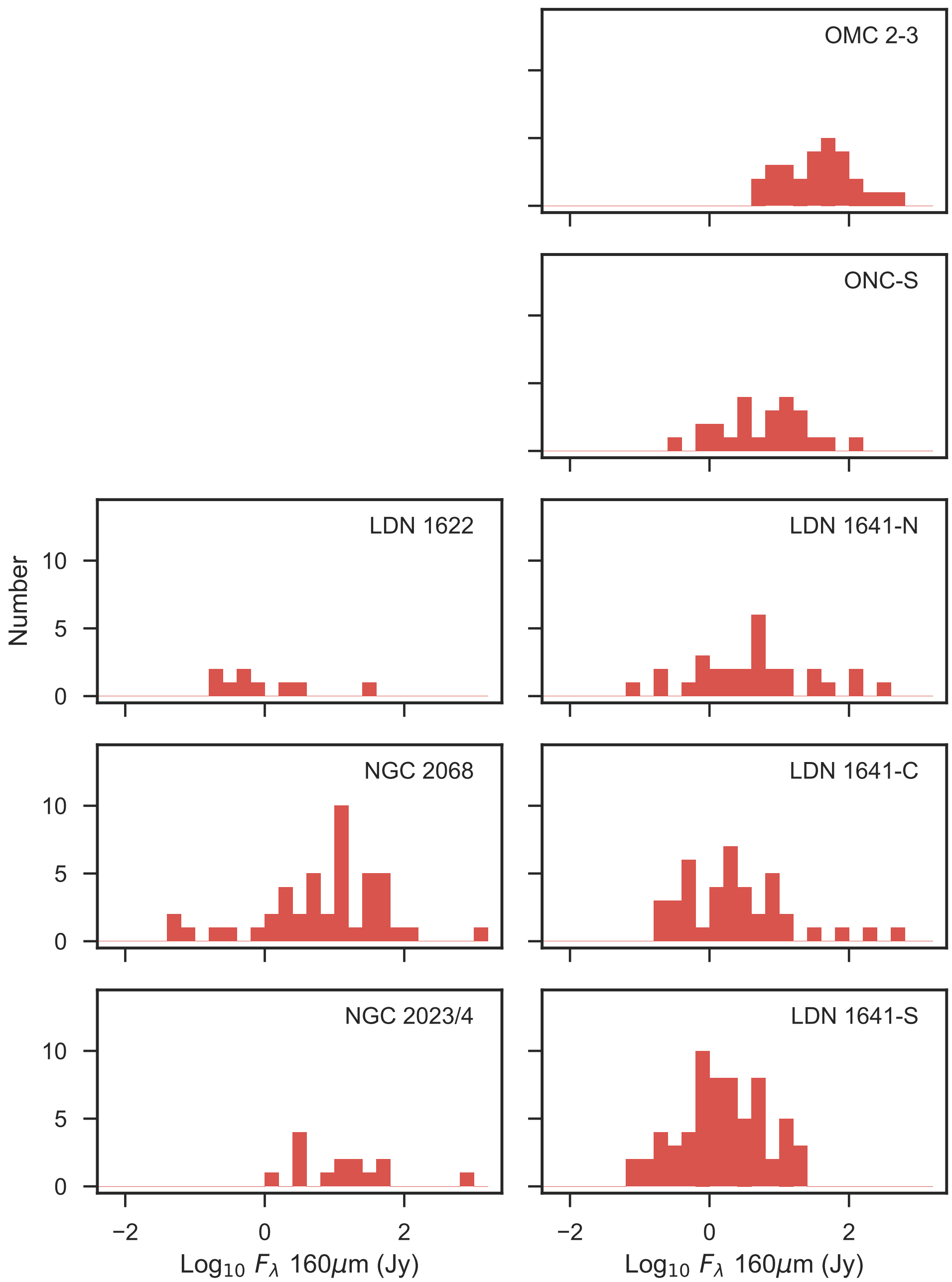

Figure 3. The 160μm flux distributions segregated by subregion for Orion B (left column) and Orion A (right column).

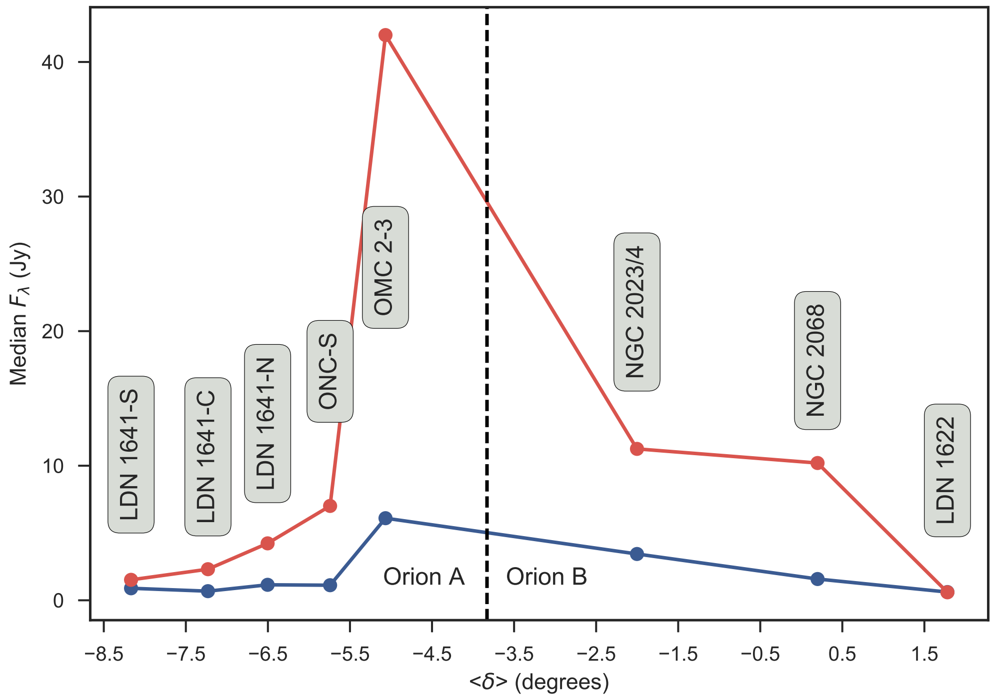

Figure 4. Median flux as a function of declination for the 70 μm FD (blue dots and curve) and the 160 μm FD (red dots and curve).

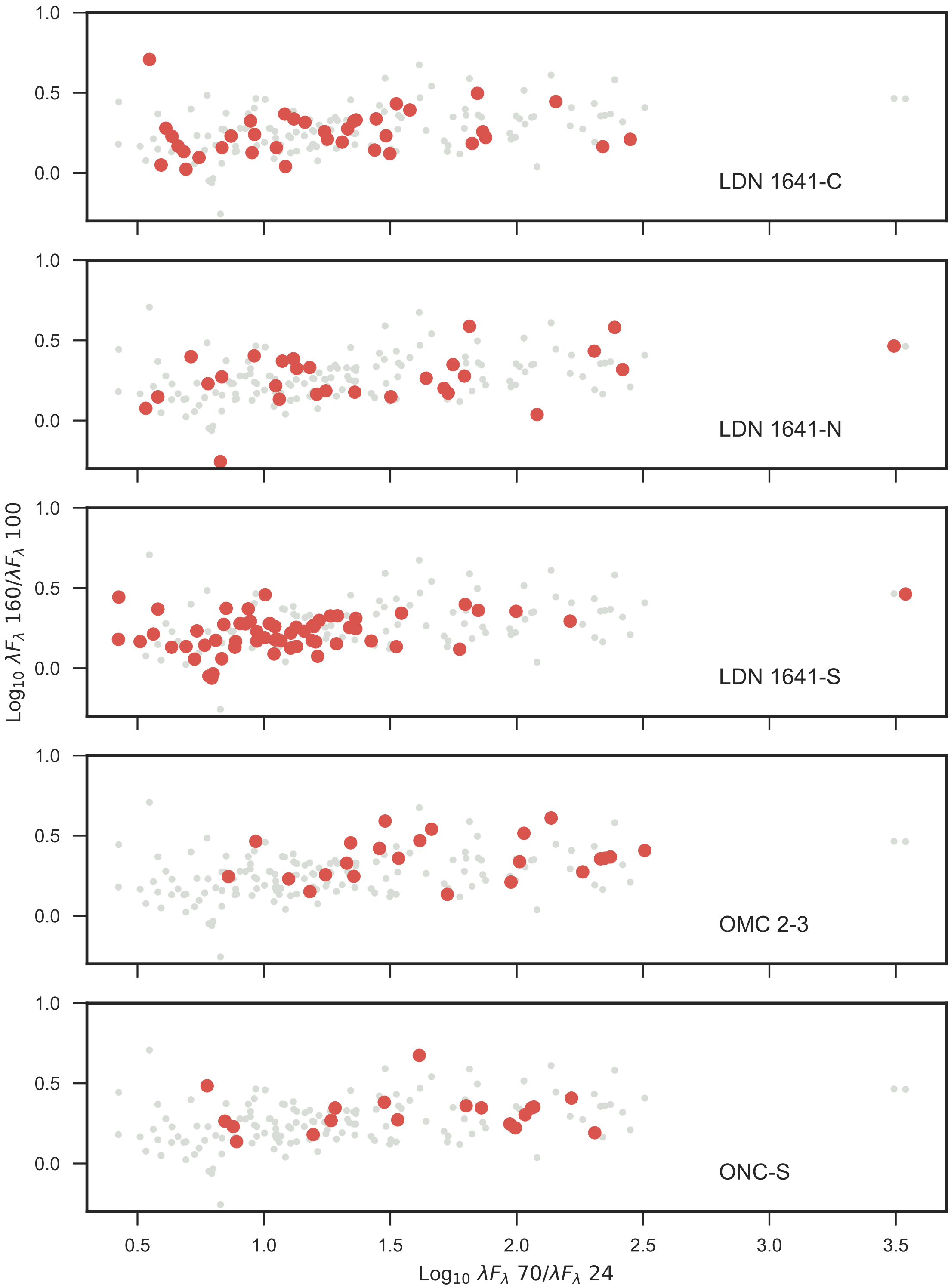

Figure 5. The observed distribution of colors in Orion A segregated by sub-regions. The sub-region is identified in the respective panel. Solid red symbols show the colors for the sub-region. Smaller black open symbols show the distribution for all sources in the combine Orion A and Orion B samples.

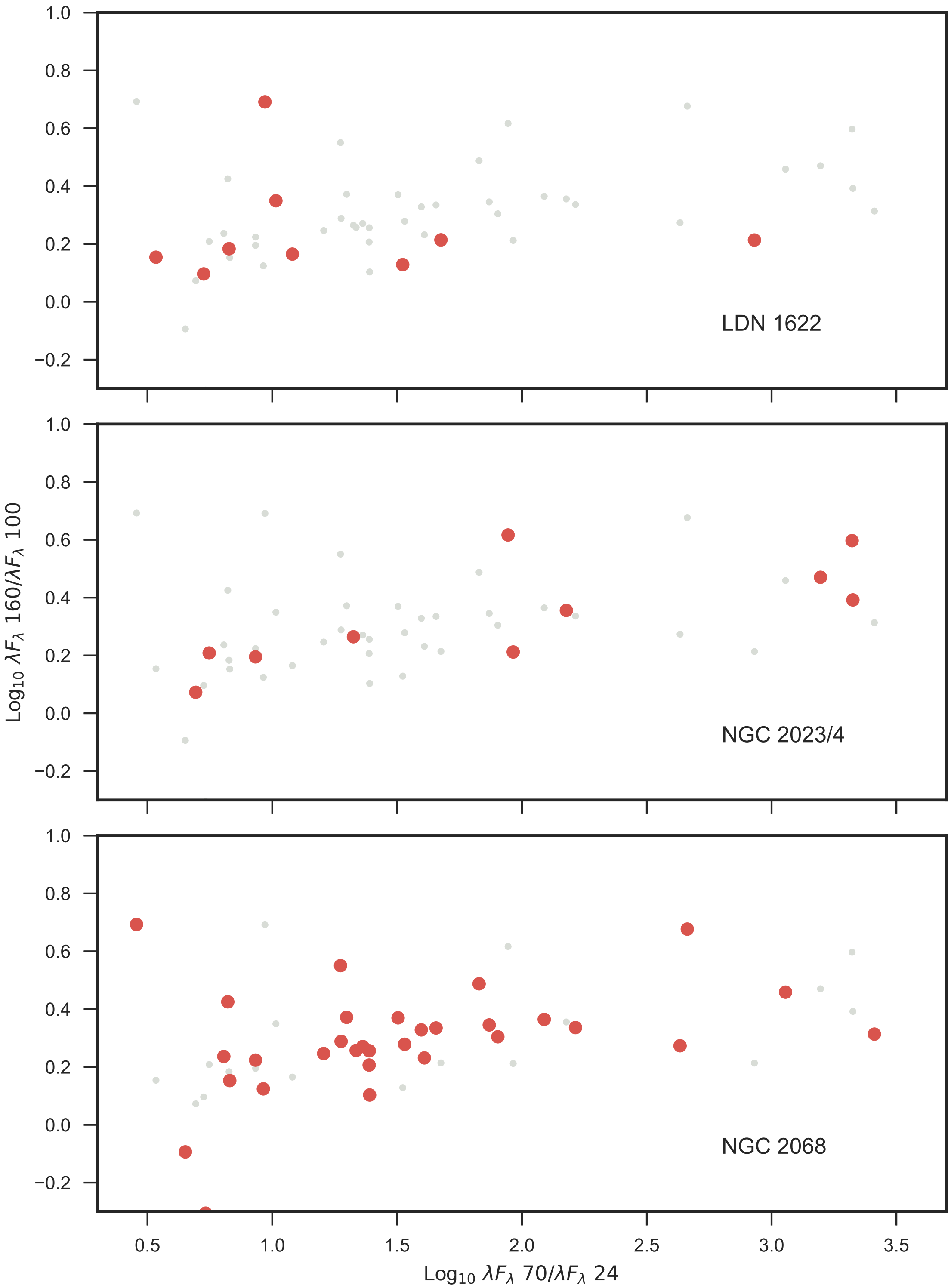

Figure 6. Same as Figure 5 for Orion B.

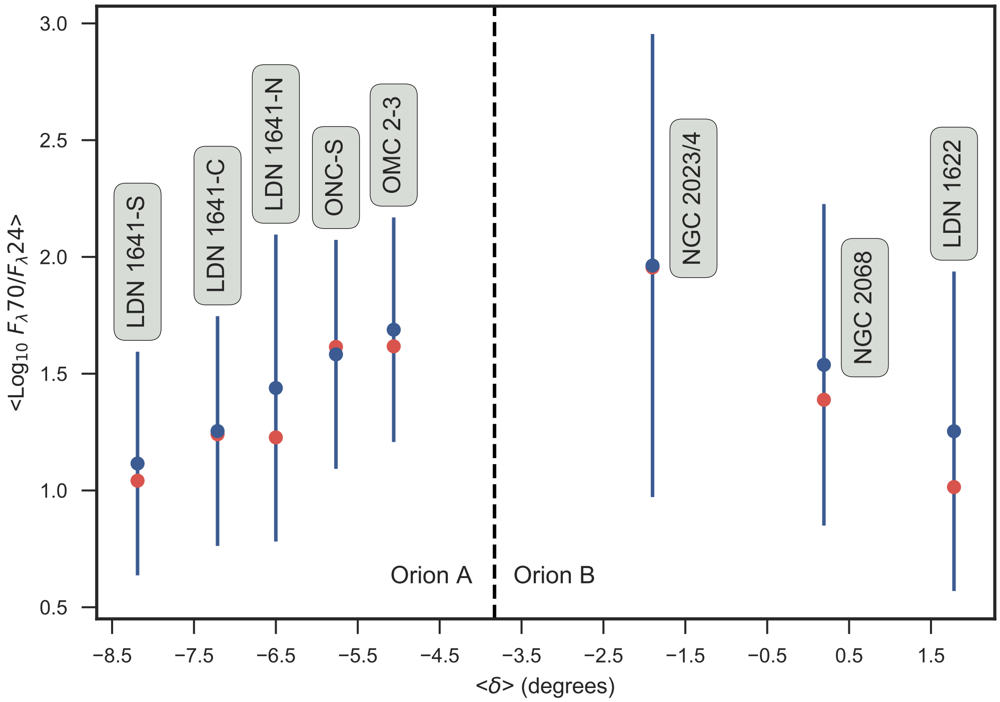

Figure 7. The mean (black circles) and median (red circles) value of $\mathrm{Log}_{10}(\lambda F_\lambda 70/\lambda F_\lambda 24)$ color as a function of declination. The associated sub-region is labelled above the data points themselves. The vertical bars show the respective standard deviation.

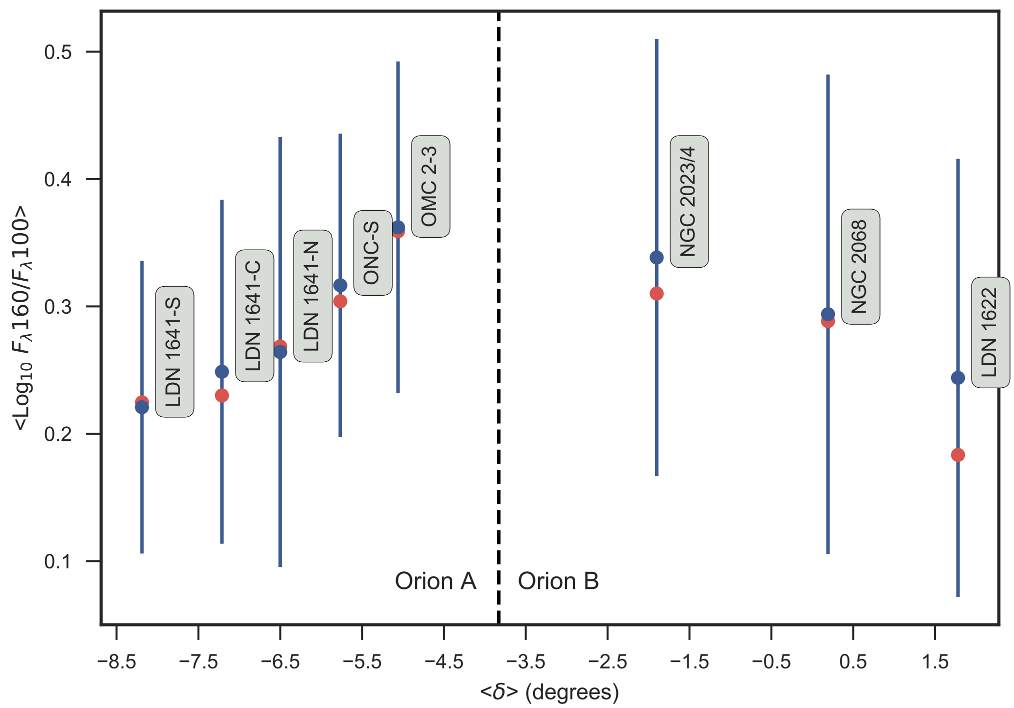

Figure 8. Same as Figure 7 for the $\mathrm{Log}_{10}(\lambda F_\lambda 160/\lambda F_\lambda 100)$ color.

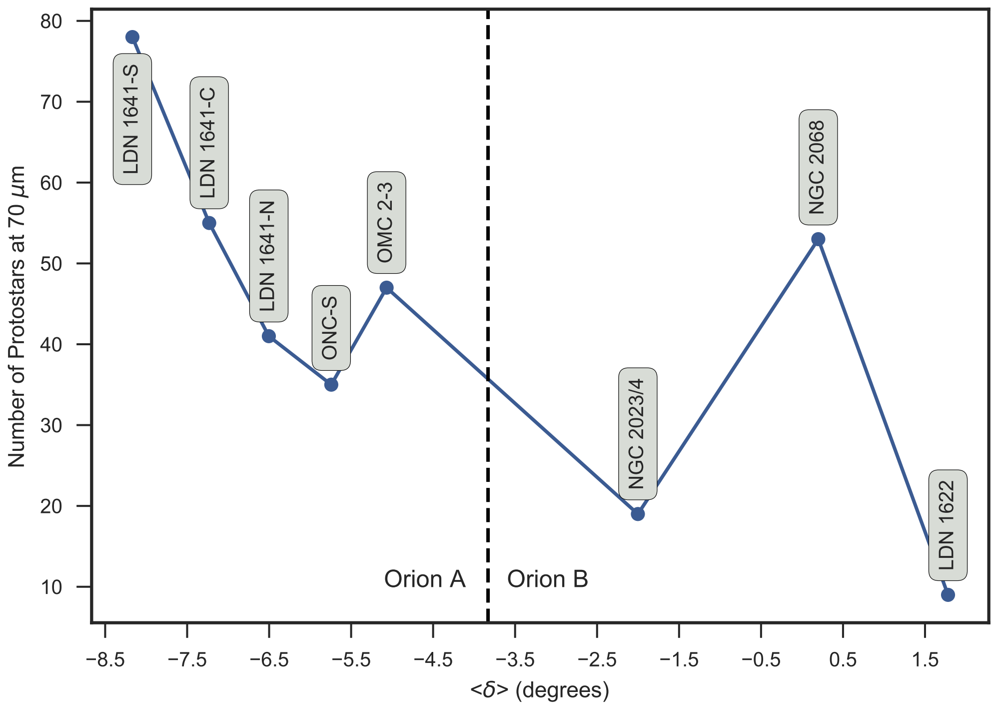

Figure 9. Number of protostars as a function of sub-region in Orion.

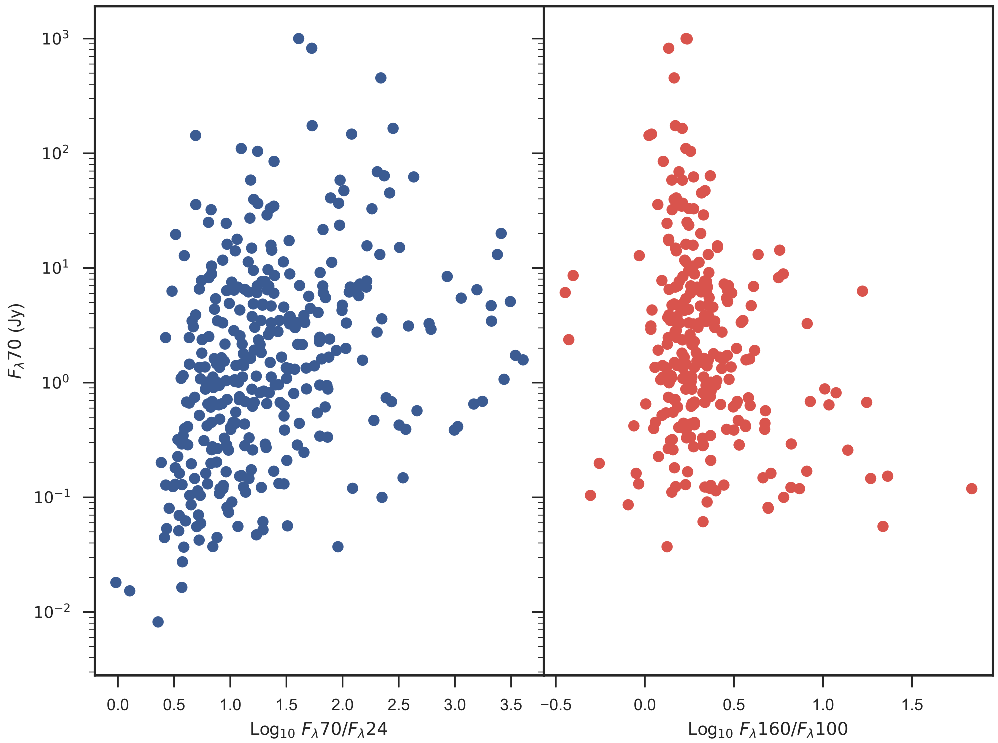

Figure 10. The observed 70 μm flux as a function of the $\mathrm{Log}_{10}(\lambda F_\lambda 70/\lambda F_\lambda 24)$ (left) and $\mathrm{Log}_{10}(\lambda F_\lambda 160/\lambda F_\lambda 100)$ (right) flux ratios.

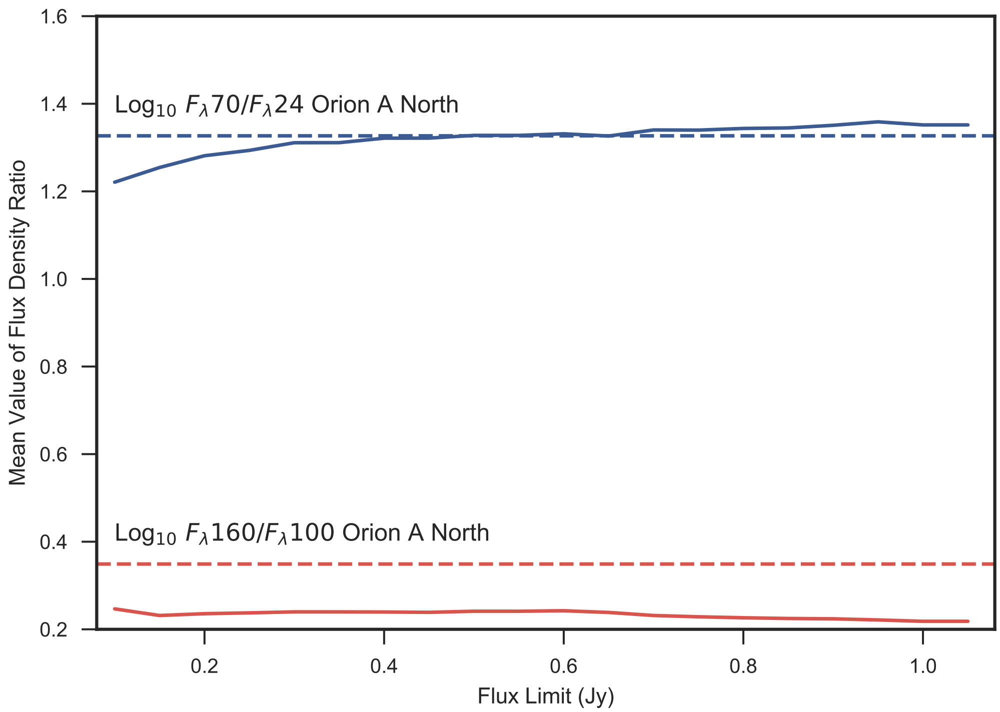

Figure 11. The observed mean color above the simulated completeness limit for LDN 1641. Solid lines show the mean values for Log$_{10}$($\lambda F_\lambda 70/\lambda F_\lambda 24$) (black) and Log$_{10}$($\lambda F_\lambda 160/\lambda F_\lambda 100$) (blue) with limiting flux. The dashed lines show the mean color for the combined Orion ONC and OMC-2/3 region. As discussed in text, we note a complete lack of correlation between the completeness limit and mean color for Log$_{10}$($\lambda F_\lambda 160/\lambda F_\lambda 100$). We note a steady increase in the mean Log$_{10}$($\lambda F_\lambda 70/\lambda F_\lambda 24$)as a function of the completeness limit. However, the average completeness limits require significant differences before the LDN 1641 sub0region can be explained as being similar to Orion OMC-2/3 and the ONC.

APPENDIX

A. HOPS CATALOG

The HOPS observational catalog.

Table 2. The HOPS observation sample

HOPS ID	α_{J2000} h:m:s	δ_{J2000} ° :′:″	Observation Identifiers	Group Number	70μm (mJy)	flag	Method	100μm (mJy)	flag	160μm (mJy)	flag	Method	Field	Observation Date (UT)
000	05:54:28.11	01:37:34.9	nan		nan	0.000	A	nan	3.000	nan	0.000	A	nan	nan
001	05:54:12.34	01:42:35.5	1342215365-66	000	3.700	1.000	A	4.570	1.000	3.840	1.000	A	LDN 1622	6 Mar 2011
002	05:54:9.13	01:42:52.0	1342215365-66	000	0.519	1.000	A	0.514	1.000	0.401	1.000	P	LDN 1622	6 Mar 2011
003	05:54:56.97	01:42:56.2	1342218780-81	001	0.319	1.000	A	0.294	1.000	0.262	1.000	A	LDN 1622	18 Apr 2011
004	05:54:53.76	01:47:10.0	1342218780-81	001	0.612	1.000	A	0.622	1.000	0.593	1.000	A	LDN 1622	18 Apr 2011
005	05:54:32.16	01:48:7.2	1342218703-04	003	0.710	1.000	A	0.753	1.000	0.688	1.000	A	LDN 1622	16 Apr 2011
006	05:54:18.41	01:49:3.4	1342218703-04	003	0.091	1.000	A	0.136	1.000	0.190	1.000	A	LDN 1622	16 Apr 2011
007	05:54:20.04	01:50:42.8	1342218703-04	003	1.340	1.000	A	1.750	1.000	1.790	1.000	A	LDN 1622	16 Apr 2011
008	05:35:33.11	-05:59:6.4	1342227328-29	006	nan	3.000	A	nan	3.000	nan	3.000	A	ONC-S	24 Aug 2011
009	05:35:49.21	-05:59:3.6	nan		nan	0.000	A	nan	3.000	nan	0.000	A	nan	nan
010	05:35:9.00	-05:58:27.6	1342204248-49	005	6.820	1.000	A	12.600	1.000	17.700	1.000	A	ONC-S	9 Sep 2010
011	05:35:13.41	-05:57:58.1	1342204248-49	005	23.600	1.000	A	33.000	1.000	36.400	1.000	A	ONC-S	9 Sep 2010
012	05:35:8.60	-05:55:54.3	1342204248-49	005	15.600	1.000	A	26.100	1.000	41.700	1.000	P	ONC-S	9 Sep 2010
013	05:35:24.56	-05:55:33.4	1342227328-29	006	1.120	1.000	A	0.932	1.000	1.070	1.000	A	ONC-S	24 Aug 2011
014	05:36:19.17	-05:55:30.3	1342227326-27	007	nan	3.000	A	nan	3.000	3.630	2.000	A	ONC-S	24 Aug 2011
015	05:36:19.02	-05:55:25.5	1342227326-27	007	0.258	1.000	A	0.340	1.000	2.930	2.000	A	ONC-S	24 Aug 2011
016	05:35:0.81	-05:55:25.7	1342204248-49	005	0.685	1.000	A	1.220	1.000	6.470	2.000	A	ONC-S	9 Sep 2010
017	05:35:7.18	-05:52:5.9	1342217446-47	008	0.673	1.000	A	0.541	1.000	5.950	2.000	A	ONC-S	30 Mar 2011
018	05:35:5.49	-05:51:54.4	1342217446-47	008	4.270	1.000	A	6.050	1.000	6.310	1.000	P	ONC-S	30 Mar 2011

Table 2 continued on next page

Table 2 *(continued)*

HOPS ID	α_{J2000} h:m:s	δ_{J2000} $^{\circ}$:$'$:$''$	Observation Identifiers	Group Number	70μm (mJy)	flag	Method	100μm (mJy)	flag	160μm (mJy)	flag	Method	Field	Observation Date (UT)
019	05:35:25.99	-05:51:22.9	1342217446-47	008	0.247	1.000	P	nan	3.000	0.953	1.000	A	ONC-S	30 Mar 2011
020	05:33:30.71	-05:50:41.0	1342217750-51	009	1.370	1.000	A	1.710	1.000	3.260	1.000	A	ONC-S	31 Mar 2011
021	05:36:10.10	-05:50:8.3	1342227096-97	010	0.119	1.000	A	0.299	2.000	1.380	2.000	A	ONC-S	22 Aug 2011
022	05:35:0.53	-05:49:2.0	1342217446-47	008	0.146	1.000	A	0.550	2.000	6.370	2.000	A	ONC-S	30 Mar 2011
023	05:36:17.89	-05:46:54.5	1342227096-97	010	nan	3.000	A	nan	3.000	nan	3.000	A	ONC-S	22 Aug 2011
024	05:34:46.94	-05:44:51.0	1342204246-47	012	0.291	1.000	A	nan	3.000	0.581	2.000	A	ONC-S	9 Sep 2010
025	05:35:22.63	-05:44:29.5	1342227098-99	013	nan	3.000	A	nan	3.000	nan	3.000	A	ONC-S	22 Aug 2011
026	05:35:17.34	-05:42:14.5	1342227098-99	013	0.130	1.000	A	nan	3.000	2.300	2.000	A	ONC-S	22 Aug 2011
027	05:36:21.72	-05:41:58.1	nan		nan	0.000	A	0.493	1.000	nan	0.000	A	nan	nan
028	05:34:47.29	-05:41:55.9	1342204246-47	012	0.945	1.000	A	1.850	1.000	2.570	1.000	P	ONC-S	9 Sep 2010
029	05:34:49.04	-05:41:42.2	1342204246-47	012	3.770	1.000	A	4.120	1.000	3.900	1.000	P	ONC-S	9 Sep 2010
030	05:34:44.06	-05:41:25.9	1342204246-47	012	7.610	1.000	A	9.370	1.000	13.000	1.000	P	ONC-S	9 Sep 2010
031	05:35:17.25	-05:40:26.9	1342227098-99	013	nan	3.000	A	nan	3.000	nan	3.000	A	ONC-S	22 Aug 2011
032	05:34:35.45	-05:39:59.1	1342204244-45	014	6.170	1.000	A	5.550	1.000	7.710	1.000	P	ONC-S	9 Sep 2010
033	05:34:45.21	-05:39:56.8	1342204246-47	012	0.108	1.000	A	nan	3.000	0.751	2.000	A	ONC-S	9 Sep 2010
034	05:35:10.90	-05:39:30.7	1342205234-35	015	nan	3.000	A	nan	3.000	nan	3.000	A	ONC-S	28 Sep 2010
035	05:35:19.93	-05:39:1.2	1342205234-35	015	nan	3.000	A	nan	3.000	nan	3.000	A	ONC-S	28 Sep 2010
036	05:34:26.43	-05:37:40.5	1342204244-45	014	0.997	1.000	A	1.020	1.000	0.872	1.000	A	ONC-S	9 Sep 2010
037	05:34:47.67	-05:37:25.2	1342204244-45	014	nan	3.000	A	nan	3.000	nan	3.000	A	ONC-S	9 Sep 2010
038	05:35:4.72	-05:37:12.3	1342205234-35	015	0.272	1.000	P	nan	3.000	17.000	2.000	A	ONC-S	28 Sep 2010
039	05:36:22.43	-05:36:24.8	nan		nan	0.000	A	0.445	1.000	nan	0.000	A	nan	nan

Table 2 continued on next page

Table 2 *(continued)*

HOPS ID	α_{J2000} h:m:s	δ_{J2000} ° :′:″	Observation Identifiers	Group Number	70μm (mJy)	flag	Method	100μm (mJy)	flag	160μm (mJy)	flag	Method	Field	Observation Date (UT)
040	05:35:8.52	-05:35:59.4	1342205234-35	015	3.310	1.000	A	11.600	1.000	14.600	1.000	P	ONC-S	28 Sep 2010
041	05:34:29.44	-05:35:42.7	1342204244-45	014	4.560	1.000	A	7.040	1.000	10.600	1.000	A	ONC-S	9 Sep 2010
042	05:35:5.04	-05:35:40.7	1342205234-35	015	1.310	1.000	A	nan	3.000	28.800	2.000	A	ONC-S	28 Sep 2010
043	05:35:4.50	-05:35:14.4	1342205234-35	015	3.250	1.000	P	14.700	1.000	17.200	1.000	P	ONC-S	28 Sep 2010
044	05:35:10.57	-05:35:6.3	1342205234-35	015	0.956	1.000	P	nan	3.000	13.000	1.000	A	ONC-S	28 Sep 2010
045	05:35:6.45	-05:33:35.1	1342205234-35	015	6.550	1.000	P	nan	3.000	8.530	1.000	A	ONC-S	28 Sep 2010
046	05:34:42.20	-05:33:3.3	1342217448-49	016	nan	3.000	A	nan	3.000	6.330	2.000	A	ONC-S	30 Mar 2011
047	05:33:45.87	-05:32:58.1	1342204433-34	308	0.018	1.000	A	nan	3.000	0.490	2.000	A	ONC-S	13 Sep 2010
048	05:35:6.56	-05:32:51.6	1342205234-35	015	5.670	2.000	A	nan	3.000	nan	3.000	A	ONC-S	28 Sep 2010
049	05:34:48.88	-05:31:45.9	1342217448-49	016	0.664	1.000	A	nan	3.000	0.622	2.000	A	ONC-S	30 Mar 2011
050	05:34:40.91	-05:31:44.4	1342217448-49	016	9.110	1.000	A	14.200	1.000	20.300	1.000	A	ONC-S	30 Mar 2011
051	05:35:15.83	-05:30:5.5	1342217450-51	017	nan	3.000	A	nan	3.000	nan	3.000	A	ONC-S	30 Mar 2011
052	05:35:16.32	-05:29:32.6	1342217450-51	017	nan	3.000	A	nan	3.000	nan	3.000	A	ONC-S	30 Mar 2011
053	05:33:57.37	-05:23:30.4	1342217752-53	018	69.000	1.000	A	106.000	1.000	103.000	1.000	A	ONC-S	31 Mar 2011
054	05:33:22.48	-05:23:2.9	nan		nan	0.000	A	nan	3.000	nan	0.000	A	nan	nan
055	05:33:54.09	-05:21:49.5	1342217752-53	018	nan	3.000	A	nan	3.000	1.230	1.000	A	ONC-S	31 Mar 2011
056	05:35:19.47	-05:15:32.7	1342205232-33	200	47.200	1.000	A	94.100	1.000	128.000	1.000	P	OMC 2-3	28 Sep 2010
057	05:35:19.84	-05:15:8.5	1342205232-33	200	4.910	1.000	A	nan	3.000	75.100	2.000	A	OMC 2-3	28 Sep 2010
058	05:35:18.51	-05:13:38.2	1342205232-33	200	3.460	1.000	A	nan	3.000	3.810	2.000	A	OMC 2-3	28 Sep 2010
059	05:35:20.14	-05:13:15.5	1342205232-33	200	58.400	1.000	A	65.600	1.000	58.100	1.000	P	OMC 2-3	28 Sep 2010
060	05:35:23.33	-05:12:3.1	1342205228-29	130	58.300	1.000	A	83.400	1.000	84.600	1.000	A	OMC 2-3	28 Sep 2010

Table 2 continued on next page

Table 2 *(continued)*

HOPS ID	α_{J2000} h:m:s	δ_{J2000} $^{\circ}$:$'$:$''$	Observation Identifiers	Group Number	70μm (mJy)	flag	Method	100μm (mJy)	flag	160μm (mJy)	flag	Method	Field	Observation Date (UT)
061	05:33:25.91	-05:12:2.6	nan		nan	0.000	A	nan	3.000	nan	0.000	A	nan	nan
062	05:35:24.58	-05:11:29.7	1342205228-29	130	nan	3.000	A	nan	3.000	44.000	2.000	A	OMC 2-3	28 Sep 2010
063	05:35:24.90	-05:10:1.5	1342205228-29	130	nan	3.000	A	nan	3.000	nan	3.000	A	OMC 2-3	28 Sep 2010
064	05:35:27.00	-05:09:54.1	1342205228-29	130	nan	3.000	A	nan	3.000	nan	3.000	A	OMC 2-3	28 Sep 2010
065	05:35:21.55	-05:09:38.7	1342205228-29	130	0.481	1.000	A	nan	3.000	28.400	2.000	A	OMC 2-3	28 Sep 2010
066	05:35:26.84	-05:09:24.6	1342205228-29	130	27.200	1.000	P	nan	3.000	325.000	2.000	A	OMC 2-3	28 Sep 2010
067	05:35:22.69	-05:08:34.0	1342205228-29	130	nan	3.000	A	nan	3.000	nan	3.000	A	OMC 2-3	28 Sep 2010
068	05:35:24.30	-05:08:30.6	1342205228-29	130	6.960	1.000	A	14.300	1.000	25.500	1.000	A	OMC 2-3	28 Sep 2010
069	05:35:25.22	-05:08:24.0	1342205228-29	130	nan	3.000	A	nan	3.000	15.600	2.000	A	OMC 2-3	28 Sep 2010
070	05:35:22.41	-05:08:4.8	1342205228-29	130	6.410	1.000	P	nan	3.000	11.600	1.000	A	OMC 2-3	28 Sep 2010
071	05:35:25.61	-05:07:57.3	1342205228-29	130	14.300	1.000	A	13.100	1.000	46.800	2.000	A	OMC 2-3	28 Sep 2010
072	05:35:25.71	-05:07:46.4	1342205228-29	130	nan	3.000	A	nan	3.000	nan	3.000	A	OMC 2-3	28 Sep 2010
073	05:35:27.70	-05:07:3.5	1342205226-27	135	1.670	1.000	A	7.110	1.000	11.700	1.000	A	OMC 2-3	28 Sep 2010
074	05:35:24.86	-05:06:21.4	1342205228-29	130	1.010	1.000	A	nan	3.000	23.800	2.000	A	OMC 2-3	28 Sep 2010
075	05:35:26.66	-05:06:10.3	1342205226-27	135	7.030	1.000	A	11.900	1.000	21.900	1.000	P	OMC 2-3	28 Sep 2010
076	05:35:25.75	-05:05:57.9	1342205226-27	135	2.160	1.000	P	nan	3.000	9.740	1.000	A	OMC 2-3	28 Sep 2010
077	05:35:31.53	-05:05:47.3	1342205226-27	135	8.870	1.000	A	9.090	1.000	34.000	2.000	A	OMC 2-3	28 Sep 2010
078	05:35:25.82	-05:05:43.7	1342205226-27	135	15.100	1.000	A	35.500	1.000	56.700	1.000	P	OMC 2-3	28 Sep 2010
079	05:35:27.88	-05:05:36.3	1342205228-29	130	nan	3.000	A	nan	3.000	nan	3.000	A	OMC 2-3	28 Sep 2010
080	05:35:25.19	-05:05:9.5	1342205226-27	135	0.155	1.000	A	nan	3.000	nan	3.000	A	OMC 2-3	28 Sep 2010
081	05:35:27.95	-05:04:58.2	1342205226-27	135	1.990	1.000	A	4.030	1.000	8.240	1.000	A	OMC 2-3	28 Sep 2010

Table 2 continued on next page

Table 2 *(continued)*

HOPS ID	α_{J2000} h:m:s	δ_{J2000} ° :′:″	Observation Identifiers	Group Number	70μm (mJy)	flag	Method	100μm (mJy)	flag	160μm (mJy)	flag	Method	Field	Observation Date (UT)
082	05:35:19.73	-05:04:54.6	1342205226-27	135	3.780	1.000	P	7.280	1.000	10.400	1.000	A	OMC 2-3	28 Sep 2010
083	05:35:55.73	-05:04:37.6	nan		nan	0.000	A	nan	3.000	nan	0.000	A	nan	nan
084	05:35:26.57	-05:03:55.1	1342205226-27	135	104.000	1.000	A	117.000	1.000	132.000	1.000	A	OMC 2-3	28 Sep 2010
085	05:35:28.18	-05:03:40.9	1342205226-27	135	29.000	1.000	A	36.000	1.000	48.000	1.000	P	OMC 2-3	28 Sep 2010
086	05:35:23.65	-05:01:40.3	1342204250-51	019	6.100	1.000	P	86.500	2.000	19.300	2.000	A	OMC 2-3	10 Sep 2010
087	05:35:23.47	-05:01:28.7	1342204250-51	019	63.600	1.000	P	158.000	1.000	230.000	1.000	P	OMC 2-3	10 Sep 2010
088	05:35:22.43	-05:01:14.2	1342204250-51	019	32.800	1.000	A	69.500	1.000	81.600	1.000	P	OMC 2-3	10 Sep 2010
089	05:35:19.96	-05:01:2.6	1342204250-51	019	3.340	1.000	A	nan	3.000	29.600	2.000	A	OMC 2-3	10 Sep 2010
090	05:35:34.47	-05:00:52.0	1342204250-51	019	2.370	1.000	A	1.780	1.000	0.416	2.000	A	OMC 2-3	10 Sep 2010
091	05:35:18.91	-05:00:50.9	1342204250-51	019	3.350	1.000	P	15.800	1.000	34.300	1.000	P	OMC 2-3	10 Sep 2010
092	05:35:18.32	-05:00:33.0	1342204250-51	019	33.000	1.000	A	51.000	1.000	56.200	1.000	P	OMC 2-3	10 Sep 2010
093	05:35:15.03	-05:00:8.2	1342204250-51	019	2.490	1.000	A	nan	3.000	49.000	2.000	A	OMC 2-3	10 Sep 2010
094	05:35:16.15	-05:00:2.3	1342204250-51	019	6.340	1.000	A	18.000	1.000	32.800	1.000	P	OMC 2-3	10 Sep 2010
095	05:35:34.20	-04:59:52.2	1342204250-51	019	0.632	1.000	P	2.420	1.000	5.900	1.000	P	OMC 2-3	10 Sep 2010
096	05:35:29.72	-04:58:48.8	1342204250-51	019	6.900	1.000	A	20.100	1.000	51.200	1.000	A	OMC 2-3	10 Sep 2010
097	05:35:28.89	-04:57:38.9	1342204250-51	019	nan	3.000	A	nan	3.000	nan	3.000	A	OMC 2-3	10 Sep 2010
098	05:35:19.32	-04:55:44.9	1342204250-51	019	1.650	1.000	P	nan	3.000	4.640	2.000	A	OMC 2-3	10 Sep 2010
099	05:34:29.50	-04:55:30.6	1342217754-55	021	3.600	1.000	A	6.190	1.000	8.850	1.000	A	OMC 2-3	31 Mar 2011
100	05:34:21.39	-04:55:14.8	1342217754-55	021	0.015	1.000	A	nan	3.000	2.330	2.000	A	OMC 2-3	31 Mar 2011
101	05:35:8.22	-04:54:9.7	1342217758-59	020	2.840	1.000	A	nan	3.000	48.100	2.000	A	OMC 2-3	31 Mar 2011
102	05:34:35.18	-04:52:17.9	1342217754-55	021	0.640	1.000	A	0.693	1.000	4.680	2.000	A	OMC 2-3	31 Mar 2011

Table 2 continued on next page

Table 2 *(continued)*

HOPS ID	α_{J2000} h:m:s	δ_{J2000} ° :′:″	Observation Identifiers	Group Number	70μm (mJy)	flag	Method	100μm (mJy)	flag	160μm (mJy)	flag	Method	Field	Observation Date (UT)
103	05:34:12.19	-04:50:7.0	1342217754-55	021	nan	3.000	A	nan	3.000	nan	3.000	A	OMC 2-3	31 Mar 2011
104	05:35:6.78	-04:50:1.8	1342217758-59	020	nan	3.000	A	nan	3.000	nan	3.000	A	OMC 2-3	31 Mar 2011
105	05:35:32.28	-04:46:48.5	1342191970-71	306	0.259	1.000	A	nan	3.000	1.130	2.000	A	OMC 2-3	10 Mar 2010
106	05:36:12.43	-04:45:15.7	nan		nan	0.000	A	nan	3.000	nan	0.000	A	nan	nan
107	05:35:23.34	-04:40:10.5	1342217756-57	024	4.370	1.000	A	5.060	1.000	5.560	1.000	A	OMC 2-3	31 Mar 2011
108	05:35:27.07	-05:10:0.4	1342205228-29	130	40.800	1.000	P	288.000	2.000	270.000	1.000	P	OMC 2-3	28 Sep 2010
109	05:35:8.56	-05:35:59.2	1342205234-35	015	nan	0.000	A	nan	0.000	nan	0.000	A	ONC-S	28 Sep 2010
110	05:36:2.23	-05:02:49.8	nan		nan	0.000	A	nan	3.000	nan	0.000	A	nan	nan
111	05:35:23.36	-05:12:2.8	1342205226-27	135	nan	0.000	A	nan	0.000	nan	0.000	A	OMC 2-3	28 Sep 2010
112	05:40:43.99	-07:22:42.9	nan		nan	0.000	A	nan	3.000	nan	0.000	A	nan	nan
113	05:39:58.13	-07:26:41.2	1342215589-90	025	0.059	1.000	A	nan	3.000	0.256	2.000	A	LDN 1641-C	7 Mar 2011
114	05:40:1.37	-07:25:38.6	1342215589-90	025	0.111	1.000	A	0.140	1.000	0.124	2.000	A	LDN 1641-C	7 Mar 2011
115	05:39:56.50	-07:25:51.5	1342215589-90	025	0.260	1.000	A	0.287	1.000	0.258	1.000	P	LDN 1641-C	7 Mar 2011
116	05:39:57.90	-07:25:13.1	1342215589-90	025	0.328	1.000	A	0.302	1.000	0.398	1.000	P	LDN 1641-C	7 Mar 2011
117	05:39:55.44	-07:24:19.5	1342215589-90	025	0.123	1.000	A	0.179	1.000	0.243	1.000	P	LDN 1641-C	7 Mar 2011
118	05:39:54.58	-07:24:14.8	1342215589-90	025	0.129	1.000	A	0.073	1.000	0.078	2.000	A	LDN 1641-C	7 Mar 2011
119	05:39:50.65	-07:23:30.4	1342215589-90	025	0.746	1.000	A	0.682	1.000	0.578	1.000	P	LDN 1641-C	7 Mar 2011
120	05:39:34.32	-07:26:11.4	1342218729-30	026	0.162	1.000	A	0.169	1.000	0.539	1.000	P	LDN 1641-C	17 Apr 2011
121	05:39:33.70	-07:23:2.0	1342227084-85	313	0.427	1.000	A	1.260	1.000	2.880	2.000	A	LDN 1641-C	22 Aug 2011
122	05:39:45.13	-07:19:13.5	1342215589-90	025	0.045	1.000	A	nan	3.000	nan	3.000	A	LDN 1641-C	7 Mar 2011
123	05:39:33.30	-07:22:57.4	1342227084-85	313	0.614	1.000	A	1.260	1.000	2.470	1.000	A	LDN 1641-C	22 Aug 2011

Table 2 continued on next page

Table 2 *(continued)*

HOPS ID	α_{J2000} h:m:s	δ_{J2000} $^\circ$:′:″	Observation Identifiers	Group Number	70μm (mJy)	flag	Method	100μm (mJy)	flag	160μm (mJy)	flag	Method	Field	Observation Date (UT)
124	05:39:19.98	-07:26:11.2	1342218729-30	026	165.000	1.000	A	233.000	1.000	236.000	1.000	A	LDN 1641-C	17 Apr 2011
125	05:39:19.61	-07:26:18.8	1342218729-30	026	21.600	1.000	P	233.000	2.000	nan	3.000	A	LDN 1641-C	17 Apr 2011
126	05:40:9.80	-07:09:53.9	nan		nan	0.000	A	nan	3.000	nan	0.000	A	nan	nan
127	05:39:0.94	-07:20:22.6	1342227086-87	028	0.754	1.000	A	0.872	1.000	1.270	1.000	A	LDN 1641-C	22 Aug 2011
128	05:38:52.01	-07:21:6.0	1342227086-87	028	0.398	1.000	P	0.738	1.000	0.517	1.000	P	LDN 1641-C	22 Aug 2011
129	05:39:11.85	-07:10:35.0	1342204252-53	029	3.490	1.000	A	4.920	1.000	4.270	1.000	P	LDN 1641-C	10 Sep 2010
130	05:39:2.96	-07:12:52.3	1342204252-53	029	2.170	1.000	A	2.930	1.000	2.450	1.000	A	LDN 1641-C	10 Sep 2010
131	05:39:7.57	-07:10:52.1	1342204252-53	029	0.386	1.000	A	0.459	1.000	0.489	1.000	A	LDN 1641-C	10 Sep 2010
132	05:39:5.36	-07:11:5.2	1342204252-53	029	0.678	1.000	A	0.562	1.000	0.667	1.000	A	LDN 1641-C	10 Sep 2010
133	05:39:5.83	-07:10:39.4	1342204252-53	029	6.980	1.000	A	8.280	1.000	9.370	1.000	A	LDN 1641-C	10 Sep 2010
134	05:38:42.78	-07:12:43.8	1342204254-55	030	3.450	1.000	A	3.580	1.000	3.290	1.000	A	LDN 1641-C	10 Sep 2010
135	05:38:45.31	-07:10:55.9	1342204254-55	030	2.360	1.000	A	2.490	1.000	2.530	1.000	A	LDN 1641-C	10 Sep 2010
136	05:38:46.54	-07:05:37.5	1342205242-43	312	1.670	1.000	A	2.030	1.000	2.110	1.000	P	LDN 1641-C	28 Sep 2010
137	05:38:53.95	-07:02:33.2	1342204256-57	031	0.037	1.000	A	nan	3.000	0.202	2.000	A	LDN 1641-C	10 Sep 2010
138	05:38:48.33	-07:02:43.4	1342205242-43	312	0.052	1.000	A	nan	3.000	1.350	2.000	A	LDN 1641-C	28 Sep 2010
139	05:38:49.62	-07:01:17.8	1342204256-57	031	6.450	1.000	A	6.250	1.000	7.360	1.000	A	LDN 1641-C	10 Sep 2010
140	05:38:46.28	-07:01:53.5	1342204256-57	031	1.120	1.000	A	1.450	1.000	1.940	1.000	P	LDN 1641-C	10 Sep 2010
141	05:38:48.01	-07:00:49.5	1342204256-57	031	0.104	1.000	A	nan	3.000	0.307	2.000	A	LDN 1641-C	10 Sep 2010
142	05:38:47.77	-07:00:26.9	1342204256-57	031	0.074	1.000	A	nan	3.000	0.985	2.000	A	LDN 1641-C	10 Sep 2010
143	05:38:46.19	-07:00:48.6	1342204256-57	031	5.390	1.000	A	6.500	1.000	6.900	1.000	A	LDN 1641-C	10 Sep 2010
144	05:38:45.01	-07:01:1.7	1342204256-57	031	4.840	1.000	P	13.400	2.000	13.600	2.000	A	LDN 1641-C	10 Sep 2010

Table 2 continued on next page

Table 2 *(continued)*

HOPS ID	α_{J2000} h:m:s	δ_{J2000} $^\circ$:$'$:$''$	Observation Identifiers	Group Number	70μm (mJy)	flag	Method	100μm (mJy)	flag	160μm (mJy)	flag	Method	Field	Observation Date (UT)
145	05:38:43.84	-07:01:13.2	1342204256-57	031	4.300	1.000	A	3.940	1.000	2.700	1.000	P	LDN 1641-C	10 Sep 2010
146	05:38:44.16	-07:00:40.4	1342204256-57	031	nan	3.000	A	nan	3.000	3.470	2.000	A	LDN 1641-C	10 Sep 2010
147	05:38:55.00	-06:56:18.6	1342204256-57	031	0.045	1.000	A	nan	3.000	0.032	2.000	A	LDN 1641-C	10 Sep 2010
148	05:38:39.51	-06:59:30.3	1342204256-57	031	0.553	1.000	A	0.466	1.000	0.419	1.000	P	LDN 1641-C	10 Sep 2010
149	05:38:40.48	-06:58:21.7	1342204256-57	031	7.770	1.000	A	7.550	1.000	5.880	1.000	A	LDN 1641-C	10 Sep 2010
150	05:38:7.53	-07:08:29.2	1342227045-46	032	6.180	1.000	A	7.410	1.000	9.580	1.000	A	LDN 1641-C	21 Aug 2011
151	05:38:42.88	-06:56:40.7	1342204256-57	031	nan	3.000	A	nan	3.000	nan	3.000	A	LDN 1641-C	10 Sep 2010
152	05:37:58.76	-07:07:25.3	1342227045-46	032	1.330	1.000	A	1.860	1.000	3.140	1.000	P	LDN 1641-C	21 Aug 2011
153	05:37:57.01	-07:06:56.5	1342227045-46	032	7.250	1.000	A	17.000	1.000	29.600	1.000	A	LDN 1641-C	21 Aug 2011
154	05:38:20.09	-06:59:4.8	1342228171-72	033	0.167	1.000	A	0.150	1.000	0.163	1.000	A	LDN 1641-C	4 Sep 2011
155	05:37:15.84	-07:17:50.0	nan		nan	0.000	A	nan	3.000	nan	0.000	A	nan	nan
156	05:38:3.40	-06:58:15.8	1342205240-41	034	0.673	1.000	A	0.773	1.000	1.050	1.000	P	LDN 1641-C	28 Sep 2010
157	05:37:56.57	-06:56:39.2	1342205240-41	034	7.620	1.000	A	11.400	1.000	11.100	1.000	A	LDN 1641-C	28 Sep 2010
158	05:37:24.46	-06:58:32.8	1342227314-15	035	1.450	1.000	A	1.400	1.000	1.480	1.000	P	LDN 1641-C	24 Aug 2011
159	05:37:53.74	-06:47:16.9	1342227088-89	036	0.227	1.000	A	0.216	1.000	0.161	1.000	A	LDN 1641-N	22 Aug 2011
160	05:37:51.04	-06:47:20.4	1342227088-89	036	2.850	1.000	A	4.110	1.000	3.860	1.000	P	LDN 1641-N	22 Aug 2011
161	05:36:34.76	-07:11:13.7	nan		nan	0.000	A	0.231	1.000	nan	0.000	A	nan	nan
162	05:36:30.97	-06:52:40.9	nan		nan	0.000	A	nan	3.000	nan	0.000	A	nan	nan
163	05:37:17.28	-06:36:18.2	1342227090-91	037	0.878	1.000	A	0.721	1.000	0.765	1.000	A	LDN 1641-N	22 Aug 2011
164	05:37:0.45	-06:37:10.5	1342227090-91	037	0.738	1.000	A	1.720	1.000	4.100	1.000	A	LDN 1641-N	22 Aug 2011
165	05:36:23.54	-06:46:14.6	1342205238-39	038	2.560	1.000	P	nan	3.000	73.400	2.000	A	LDN 1641-N	28 Sep 2010

Table 2 continued on next page

Table 2 *(continued)*

HOPS ID	α_{J2000} h:m:s	δ_{J2000} ° :′:″	Observation Identifiers	Group Number	70μm (mJy)	flag	Method	100μm (mJy)	flag	160μm (mJy)	flag	Method	Field	Observation Date (UT)
166	05:36:25.13	-06:44:41.8	1342205238-39	038	17.800	1.000	A	18.600	1.000	15.800	1.000	A	LDN 1641-N	28 Sep 2010
167	05:36:19.79	-06:46:0.9	1342205238-39	038	0.203	1.000	A	nan	3.000	4.010	2.000	A	LDN 1641-N	28 Sep 2010
168	05:36:18.93	-06:45:22.7	1342205238-39	038	147.000	1.000	A	182.000	1.000	124.000	1.000	A	LDN 1641-N	28 Sep 2010
169	05:36:36.12	-06:38:51.9	1342227094-95	040	5.090	1.000	A	15.800	1.000	28.800	1.000	A	LDN 1641-N	22 Aug 2011
170	05:36:41.33	-06:34:0.1	1342227092-93	039	1.150	1.000	A	1.030	1.000	0.905	1.000	A	LDN 1641-N	22 Aug 2011
171	05:36:17.20	-06:38:1.6	1342227094-95	040	4.440	1.000	A	6.250	1.000	6.200	1.000	P	LDN 1641-N	22 Aug 2011
172	05:36:19.44	-06:29:6.8	1342227316-17	041	1.040	1.000	P	1.250	1.000	1.980	1.000	P	LDN 1641-N	24 Aug 2011
173	05:36:26.04	-06:25:5.2	1342205236-37	042	2.150	1.000	P	4.580	1.000	5.260	1.000	P	LDN 1641-N	28 Sep 2010
174	05:36:25.86	-06:24:58.7	1342205236-37	042	1.620	1.000	P	4.580	2.000	7.930	2.000	A	LDN 1641-N	28 Sep 2010
175	05:36:24.06	-06:24:54.9	1342205236-37	042	0.286	1.000	A	4.160	2.000	8.800	2.000	A	LDN 1641-N	28 Sep 2010
176	05:36:23.58	-06:24:51.6	1342205236-37	042	0.947	1.000	P	4.160	2.000	5.730	1.000	P	LDN 1641-N	28 Sep 2010
177	05:35:50.02	-06:34:53.4	1342227310-11	043	1.090	1.000	A	1.330	1.000	1.170	1.000	P	LDN 1641-N	24 Aug 2011
178	05:36:24.61	-06:22:41.3	1342205236-37	042	36.500	1.000	A	42.000	1.000	40.200	1.000	A	LDN 1641-N	28 Sep 2010
179	05:36:21.84	-06:23:29.8	1342205236-37	042	1.790	1.000	A	2.550	1.000	3.870	1.000	P	LDN 1641-N	28 Sep 2010
180	05:36:59.39	-06:10:15.6	nan		nan	0.000	A	nan	3.000	nan	0.000	A	nan	nan
181	05:36:19.50	-06:22:12.4	1342205236-37	042	11.300	1.000	P	286.000	2.000	nan	3.000	A	LDN 1641-N	28 Sep 2010
182	05:36:18.83	-06:22:10.2	1342205236-37	042	174.000	1.000	A	286.000	1.000	265.000	1.000	A	LDN 1641-N	28 Sep 2010
183	05:36:17.86	-06:22:28.1	1342205236-37	042	0.959	1.000	P	nan	3.000	nan	3.000	A	LDN 1641-N	28 Sep 2010
184	05:36:12.95	-06:23:30.6	1342205236-37	042	0.282	1.000	A	0.500	1.000	0.661	1.000	A	LDN 1641-N	28 Sep 2010
185	05:36:36.98	-06:14:58.0	1342204258-59	044	1.610	1.000	A	2.820	1.000	6.830	1.000	P	LDN 1641-N	10 Sep 2010
186	05:35:47.28	-06:26:14.7	1342215593-94	045	1.400	1.000	A	1.590	1.000	2.220	1.000	A	LDN 1641-N	7 Mar 2011

Table 2 continued on next page

Table 2 *(continued)*

HOPS ID	α_{J2000} h:m:s	δ_{J2000} $^{\circ}$:′:″	Observation Identifiers	Group Number	70μm (mJy)	flag	Method	100μm (mJy)	flag	160μm (mJy)	flag	Method	Field	Observation Date (UT)
187	05:35:50.94	-06:22:43.5	1342215593-94	045	0.053	1.000	A	nan	3.000	nan	3.000	A	LDN 1641-N	7 Mar 2011
188	05:35:29.82	-06:26:58.2	1342215593-94	045	39.600	1.000	A	37.600	1.000	34.300	1.000	A	LDN 1641-N	7 Mar 2011
189	05:35:30.89	-06:26:32.1	1342215593-94	045	1.630	1.000	A	3.620	1.000	4.850	1.000	P	LDN 1641-N	7 Mar 2011
190	05:35:28.50	-06:27:1.8	1342215593-94	045	0.201	1.000	P	nan	3.000	5.880	2.000	A	LDN 1641-N	7 Mar 2011
191	05:36:17.26	-06:11:11.0	1342227324-25	047	1.010	1.000	A	1.070	1.000	1.570	1.000	P	LDN 1641-N	24 Aug 2011
192	05:36:32.45	-06:01:16.2	1342217444-45	048	2.150	1.000	A	3.230	1.000	3.740	1.000	P	ONC-S	30 Mar 2011
193	05:36:30.27	-06:01:17.4	1342217444-45	048	1.460	1.000	A	1.610	1.000	1.710	1.000	P	ONC-S	30 Mar 2011
194	05:35:52.00	-06:10:1.8	1342227322-23	049	10.400	1.000	A	10.500	1.000	12.300	1.000	A	LDN 1641-N	24 Aug 2011
195	05:36:0.06	-06:07:14.2	1342227322-23	049	nan	3.000	A	nan	3.000	nan	3.000	A	LDN 1641-N	24 Aug 2011
196	05:35:20.91	-06:18:22.3	nan		nan	0.000	A	0.180	1.000	nan	0.000	A	nan	nan
197	05:34:15.88	-06:34:32.7	1342217748-49	050	0.198	1.000	A	0.189	1.000	0.065	1.000	A	LDN 1641-N	31 Mar 2011
198	05:35:22.18	-06:13:6.2	1342227318-19	051	2.280	1.000	A	3.570	1.000	4.230	1.000	P	LDN 1641-N	24 Aug 2011
199	05:34:39.86	-06:25:14.2	1342203649-50	311	0.114	1.000	A	0.117	1.000	0.183	1.000	P	LDN 1641-N	26 Aug 2010
200	05:35:33.21	-06:06:9.6	1342227320-21	052	0.443	1.000	A	0.437	1.000	0.450	1.000	A	LDN 1641-N	24 Aug 2011
201	05:34:6.94	-06:32:8.0	1342217748-49	050	0.070	1.000	A	nan	3.000	0.701	2.000	A	LDN 1641-N	31 Mar 2011
202	05:33:43.92	-06:13:46.2	nan		nan	0.000	A	nan	3.000	nan	0.000	A	nan	nan
203	05:36:22.84	-06:46:6.2	1342205238-39	038	45.100	1.000	A	80.700	1.000	105.000	1.000	A	LDN 1641-N	28 Sep 2010
204	05:43:10.18	-08:46:7.9	1342218735-36	053	3.410	1.000	A	4.500	1.000	6.200	1.000	A	LDN 1641-S	17 Apr 2011
205	05:43:2.88	-08:47:49.4	1342218735-36	053	0.062	1.000	A	nan	3.000	0.753	2.000	A	LDN 1641-S	17 Apr 2011
206	05:43:7.26	-08:44:31.1	1342218735-36	053	5.510	1.000	P	6.330	1.000	9.080	1.000	P	LDN 1641-S	17 Apr 2011
207	05:42:38.58	-08:50:18.6	1342218796-97	054	0.346	1.000	A	0.465	1.000	0.679	1.000	A	LDN 1641-S	18 Apr 2011

Table 2 continued on next page

Table 2 *(continued)*

HOPS ID	α_{J2000} h:m:s	δ_{J2000} $^{\circ}$:$'$:$''$	Observation Identifiers	Group Number	70μm (mJy)	flag	Method	100μm (mJy)	flag	160μm (mJy)	flag	Method	Field	Observation Date (UT)
208	05:42:52.72	-08:44:12.7	1342218735-36	053	0.008	1.000	A	nan	3.000	0.431	2.000	A	LDN 1641-S	17 Apr 2011
209	05:42:52.89	-08:41:41.2	1342218798-99	055	0.276	1.000	A	0.191	1.000	0.224	1.000	A	LDN 1641-S	18 Apr 2011
210	05:42:58.27	-08:38:5.4	1342205256-57	056	2.170	1.000	A	2.530	1.000	2.110	1.000	P	LDN 1641-S	28 Sep 2010
211	05:42:58.36	-08:37:43.5	1342218798-99	055	0.545	1.000	A	1.340	1.000	1.100	1.000	P	LDN 1641-S	18 Apr 2011
212	05:42:58.39	-08:37:41.6	1342205256-57	056	nan	0.000	A	nan	0.000	nan	0.000	A	LDN 1641-S	28 Sep 2010
213	05:42:48.09	-08:40:8.3	1342218798-99	055	1.080	1.000	A	1.020	1.000	1.090	1.000	A	LDN 1641-S	18 Apr 2011
214	05:42:47.22	-08:36:36.6	1342205256-57	056	0.131	1.000	A	0.165	1.000	0.095	1.000	A	LDN 1641-S	28 Sep 2010
215	05:43:9.58	-08:29:27.1	1342218788-89	058	1.020	1.000	A	0.864	1.000	0.982	1.000	A	LDN 1641-S	18 Apr 2011
216	05:42:55.54	-08:32:48.3	1342218794-95	059	1.410	1.000	A	1.370	1.000	1.300	1.000	P	LDN 1641-S	18 Apr 2011
217	05:43:11.16	-08:24:20.1	nan		nan	0.000	A	nan	3.000	nan	0.000	A	nan	nan
218	05:43:9.90	-08:13:23.5	nan		nan	0.000	A	nan	3.000	nan	0.000	A	nan	nan
219	05:41:29.25	-08:43:4.3	1342215359-60	060	4.740	1.000	A	4.880	1.000	4.330	1.000	A	LDN 1641-S	6 Mar 2011
220	05:41:29.78	-08:42:46.0	1342215359-60	060	0.407	1.000	P	0.471	1.000	0.456	1.000	A	LDN 1641-S	6 Mar 2011
221	05:42:47.05	-08:17:7.0	1342205254-55	061	14.900	1.000	A	16.800	1.000	15.600	1.000	A	LDN 1641-S	28 Sep 2010
222	05:41:26.68	-08:42:24.5	1342215359-60	060	0.420	1.000	A	0.474	1.000	0.257	1.000	P	LDN 1641-S	6 Mar 2011
223	05:42:48.46	-08:16:34.5	1342205254-55	061	16.100	1.000	A	19.500	1.000	20.700	1.000	A	LDN 1641-S	28 Sep 2010
224	05:41:32.03	-08:40:9.7	1342215359-60	060	6.810	1.000	A	11.800	1.000	14.500	1.000	A	LDN 1641-S	6 Mar 2011
225	05:41:30.35	-08:40:17.6	1342215359-60	060	0.652	1.000	P	1.240	2.000	0.784	1.000	A	LDN 1641-S	6 Mar 2011
226	05:41:30.06	-08:40:9.4	1342215359-60	060	1.060	1.000	P	1.300	1.000	0.997	1.000	P	LDN 1641-S	6 Mar 2011
227	05:41:32.33	-08:37:55.5	1342218790-91	117	0.429	1.000	A	0.351	1.000	0.416	1.000	A	LDN 1641-S	18 Apr 2011
228	05:41:34.17	-08:35:27.7	1342218790-91	117	14.100	1.000	A	14.600	1.000	13.700	1.000	A	LDN 1641-S	18 Apr 2011

Table 2 continued on next page

Table 2 *(continued)*

HOPS ID	α_{J2000} h:m:s	δ_{J2000} $^{\circ}$:′:″	Observation Identifiers	Group Number	70μm (mJy)	flag	Method	100μm (mJy)	flag	160μm (mJy)	flag	Method	Field	Observation Date (UT)
229	05:42:47.37	-08:10:8.8	1342218792-93	062	0.128	1.000	A	0.174	1.000	0.302	1.000	P	LDN 1641-S	18 Apr 2011
230	05:42:30.80	-08:09:5.3	nan		nan	0.000	A	nan	3.000	nan	0.000	A	nan	nan
231	05:40:28.54	-08:32:55.1	nan		nan	0.000	A	nan	3.000	nan	0.000	A	nan	nan
232	05:41:35.45	-08:08:22.5	1342218800-01	063	1.090	1.000	A	0.727	1.000	0.742	1.000	P	LDN 1641-S	18 Apr 2011
233	05:41:52.31	-08:01:22.0	1342205252-53	064	0.122	1.000	A	0.170	1.000	0.702	2.000	A	LDN 1641-S	28 Sep 2010
234	05:41:49.95	-08:01:26.5	1342205252-53	064	4.860	1.000	A	5.720	1.000	5.220	1.000	P	LDN 1641-S	28 Sep 2010
235	05:41:25.34	-08:05:54.8	1342205250-51	118	2.470	1.000	A	2.260	1.000	1.910	1.000	A	LDN 1641-S	28 Sep 2010
236	05:41:30.21	-08:03:41.5	1342205250-51	118	6.510	1.000	A	7.080	1.000	6.050	1.000	A	LDN 1641-S	28 Sep 2010
237	05:41:28.97	-08:03:25.8	1342205250-51	118	0.450	1.000	P	0.494	1.000	0.586	1.000	P	LDN 1641-S	28 Sep 2010
238	05:41:26.64	-08:03:12.6	1342205250-51	118	0.451	1.000	A	0.429	1.000	0.307	1.000	P	LDN 1641-S	28 Sep 2010
239	05:41:27.06	-08:00:54.8	1342215591-92	065	0.330	1.000	A	0.628	1.000	0.673	2.000	A	LDN 1641-S	7 Mar 2011
240	05:41:25.97	-08:01:15.9	1342215591-92	065	0.174	1.000	A	nan	3.000	0.232	2.000	A	LDN 1641-S	7 Mar 2011
241	05:41:26.40	-08:01:2.1	1342215591-92	065	1.460	1.000	P	1.690	1.000	1.750	1.000	P	LDN 1641-S	7 Mar 2011
242	05:40:48.52	-08:11:9.0	1342206322-23	119	0.181	1.000	A	0.119	1.000	0.109	1.000	A	LDN 1641-S	11 Oct 2010
243	05:41:1.66	-08:06:44.8	1342215361-62	066	0.953	1.000	A	1.140	1.000	1.780	1.000	P	LDN 1641-S	6 Mar 2011
244	05:41:1.99	-08:06:1.9	1342215361-62	066	3.320	1.000	A	4.010	1.000	4.420	1.000	A	LDN 1641-S	6 Mar 2011
245	05:41:22.86	-07:58:56.0	1342215591-92	065	0.266	1.000	A	0.239	1.000	0.202	1.000	P	LDN 1641-S	7 Mar 2011
246	05:40:47.12	-08:09:47.8	1342206322-23	119	0.817	1.000	A	0.846	1.000	1.120	1.000	A	LDN 1641-S	11 Oct 2010
247	05:41:26.22	-07:56:51.6	1342205248-49	121	4.740	1.000	A	13.000	1.000	18.400	1.000	A	LDN 1641-S	28 Sep 2010
248	05:41:22.09	-07:58:3.0	1342215591-92	065	1.360	1.000	A	1.010	1.000	0.719	1.000	P	LDN 1641-S	7 Mar 2011
249	05:40:52.86	-08:05:48.8	1342215361-62	066	0.056	1.000	A	0.074	1.000	1.010	2.000	A	LDN 1641-S	6 Mar 2011

Table 2 continued on next page

Table 2 *(continued)*

HOPS ID	α_{J2000} h:m:s	δ_{J2000} $^{\circ}$:$'$:$''$	Observation Identifiers	Group Number	70μm (mJy)	flag	Method	100μm (mJy)	flag	160μm (mJy)	flag	Method	Field	Observation Date (UT)
250	05:40:48.84	-08:06:57.2	1342215361-62	066	17.300	1.000	A	19.500	1.000	16.600	1.000	A	LDN 1641-S	6 Mar 2011
251	05:40:54.01	-08:05:13.0	1342215361-62	066	0.655	1.000	A	0.698	1.000	0.825	1.000	P	LDN 1641-S	6 Mar 2011
252	05:40:49.92	-08:06:8.3	1342215361-62	066	3.040	1.000	A	3.220	1.000	4.000	1.000	P	LDN 1641-S	6 Mar 2011
253	05:41:28.77	-07:53:51.0	1342205248-49	121	0.877	1.000	A	1.080	1.000	1.240	1.000	A	LDN 1641-S	28 Sep 2010
254	05:41:24.52	-07:55:7.3	1342205248-49	121	11.300	1.000	A	12.600	1.000	13.400	1.000	A	LDN 1641-S	28 Sep 2010
255	05:40:50.57	-08:05:48.7	1342215361-62	066	0.292	1.000	A	0.340	1.000	1.410	2.000	A	LDN 1641-S	6 Mar 2011
256	05:40:45.26	-08:06:42.2	1342215361-62	066	0.169	1.000	A	0.363	1.000	1.840	2.000	A	LDN 1641-S	6 Mar 2011
257	05:41:19.87	-07:55:46.6	1342205248-49	121	0.436	1.000	A	0.735	1.000	0.827	1.000	P	LDN 1641-S	28 Sep 2010
258	05:41:24.71	-07:54:8.5	1342205248-49	121	0.907	1.000	A	1.430	1.000	2.110	1.000	P	LDN 1641-S	28 Sep 2010
259	05:40:20.88	-08:13:55.2	1342227078-79	067	0.714	1.000	A	0.896	1.000	0.828	1.000	P	LDN 1641-S	22 Aug 2011
260	05:40:19.39	-08:14:16.4	1342227078-79	067	1.540	1.000	A	1.690	1.000	2.070	1.000	A	LDN 1641-S	22 Aug 2011
261	05:41:18.89	-07:55:29.1	1342205248-49	121	4.660	1.000	A	5.510	1.000	7.050	1.000	A	LDN 1641-S	28 Sep 2010
262	05:41:23.97	-07:53:42.0	1342205248-49	121	1.120	1.000	P	3.130	2.000	2.470	1.000	P	LDN 1641-S	28 Sep 2010
263	05:41:23.68	-07:53:46.8	1342205248-49	121	1.140	1.000	P	3.130	2.000	3.490	1.000	P	LDN 1641-S	28 Sep 2010
264	05:40:59.11	-08:00:14.3	1342215361-62	066	0.056	1.000	A	nan	3.000	0.041	2.000	A	LDN 1641-S	6 Mar 2011
265	05:41:20.32	-07:53:10.6	1342205248-49	121	0.070	1.000	A	nan	3.000	1.920	2.000	A	LDN 1641-S	28 Sep 2010
266	05:41:11.81	-07:53:35.8	1342205248-49	121	0.061	1.000	A	0.076	1.000	0.101	1.000	A	LDN 1641-S	28 Sep 2010
267	05:41:19.66	-07:50:41.0	1342227848-49	068	1.500	1.000	A	1.440	1.000	1.320	1.000	A	LDN 1641-S	3 Sep 2011
268	05:40:38.33	-08:00:36.0	1342227080-81	069	2.790	1.000	A	2.620	1.000	2.420	1.000	A	LDN 1641-S	22 Aug 2011
269	05:41:27.01	-07:42:33.8	nan		nan	0.000	A	0.065	1.000	nan	0.000	A	nan	nan
270	05:40:40.53	-07:54:39.8	1342228167-68	070	0.622	1.000	A	0.614	1.000	0.698	1.000	P	LDN 1641-S	4 Sep 2011

Table 2 continued on next page

Table 2 *(continued)*

HOPS ID	α_{J2000} h:m:s	δ_{J2000} ° :′:″	Observation Identifiers	Group Number	70μm (mJy)	flag	Method	100μm (mJy)	flag	160μm (mJy)	flag	Method	Field	Observation Date (UT)
271	05:40:43.96	-07:49:30.4	1342228163-64	071	0.127	1.000	A	0.157	1.000	0.230	1.000	P	LDN 1641-S	4 Sep 2011
272	05:40:20.53	-07:56:39.6	1342218733-34	072	2.470	1.000	P	3.670	1.000	3.470	1.000	P	LDN 1641-S	17 Apr 2011
273	05:40:20.88	-07:56:24.7	1342218733-34	072	2.520	1.000	P	3.300	1.000	3.080	1.000	P	LDN 1641-S	17 Apr 2011
274	05:40:20.71	-07:54:59.7	1342218733-34	072	1.360	1.000	A	1.230	1.000	1.460	1.000	A	LDN 1641-S	17 Apr 2011
275	05:40:36.35	-07:49:7.0	1342228163-64	071	0.162	1.000	A	0.173	1.000	0.097	1.000	A	LDN 1641-S	4 Sep 2011
276	05:40:42.91	-07:45:1.9	1342228325-26	073	0.124	1.000	A	0.072	1.000	0.067	2.000	A	LDN 1641-S	7 Sep 2011
277	05:40:44.36	-07:44:16.7	1342228325-26	073	0.042	1.000	A	nan	3.000	0.401	2.000	A	LDN 1641-S	7 Sep 2011
278	05:40:20.35	-07:51:14.9	1342218731-32	074	0.392	1.000	A	0.335	1.000	0.602	1.000	A	LDN 1641-S	17 Apr 2011
279	05:40:17.79	-07:48:26.0	1342218731-32	074	3.900	1.000	A	3.350	1.000	2.860	1.000	A	LDN 1641-S	17 Apr 2011
280	05:40:14.93	-07:48:48.7	1342218731-32	074	6.810	1.000	A	6.520	1.000	6.040	1.000	A	LDN 1641-S	17 Apr 2011
281	05:40:24.62	-07:43:8.3	1342227082-83	075	2.620	1.000	A	3.230	1.000	3.620	1.000	A	LDN 1641-S	22 Aug 2011
282	05:40:26.09	-07:37:32.0	1342205246-47	076	1.920	1.000	A	2.130	1.000	1.580	1.000	A	LDN 1641-S	28 Sep 2010
283	05:40:44.67	-07:29:54.5	1342228327-28	077	0.414	1.000	A	nan	3.000	0.309	1.000	A	LDN 1641-C	7 Sep 2011
284	05:38:51.48	-08:01:27.4	1342228169-70	078	0.312	1.000	A	0.275	1.000	0.239	1.000	A	LDN 1641-S	4 Sep 2011
285	05:40:5.90	-07:29:32.9	1342205244-45	079	0.335	1.000	A	0.428	1.000	0.483	1.000	A	LDN 1641-C	28 Sep 2010
286	05:39:58.70	-07:31:12.1	1342205244-45	079	1.350	1.000	A	1.710	1.000	1.410	1.000	P	LDN 1641-C	28 Sep 2010
287	05:40:8.78	-07:27:27.7	1342228161-62	123	1.500	1.000	A	1.760	1.000	2.310	1.000	A	LDN 1641-C	4 Sep 2011
288	05:39:55.94	-07:30:28.0	1342205244-45	079	454.000	1.000	A	468.000	1.000	427.000	1.000	P	LDN 1641-C	28 Sep 2010
289	05:39:56.75	-07:30:6.1	1342215589-90	025	nan	3.000	A	nan	3.000	nan	3.000	A	LDN 1641-C	7 Mar 2011
290	05:39:57.41	-07:29:33.4	1342205244-45	079	3.020	1.000	A	6.460	1.000	9.970	1.000	A	LDN 1641-C	28 Sep 2010
291	05:39:57.97	-07:28:57.5	1342205244-45	079	0.119	1.000	A	0.165	1.000	7.060	2.000	A	LDN 1641-C	28 Sep 2010

Table 2 continued on next page

Table 2 *(continued)*

HOPS ID	α_{J2000} h:m:s	δ_{J2000} $^{\circ}$:′:″	Observation Identifiers	Group Number	70μm (mJy)	flag	Method	100μm (mJy)	flag	160μm (mJy)	flag	Method	Field	Observation Date (UT)
292	05:37:54.88	-07:41:20.3	nan		nan	0.000	A	0.282	1.000	nan	0.000	A	nan	nan
293	05:40:58.89	-07:48:2.1	1342228165-66	320	0.037	1.000	A	nan	3.000	0.057	2.000	A	LDN 1641-S	4 Sep 2011
294	05:40:51.72	-02:26:48.6	1342226729-30	080	1.810	1.000	P	3.040	1.000	3.070	1.000	P	NGC 2023-4	18 Aug 2011
295	05:41:28.94	-02:23:19.4	1342226733-34	081	0.656	1.000	P	1.070	1.000	1.230	1.000	P	NGC 2023-4	18 Aug 2011
296	05:41:17.17	-02:18:7.6	1342227049-50	083	nan	3.000	A	nan	3.000	nan	3.000	A	NGC 2023-4	21 Aug 2011
297	05:41:23.27	-02:17:35.8	1342228913-14	082	0.196	1.000	P	nan	3.000	8.700	2.000	A	NGC 2023-4	19 Sep 2011
298	05:41:37.17	-02:17:17.0	1342227049-50	083	35.700	1.000	A	29.100	1.000	21.500	1.000	P	NGC 2023-4	21 Aug 2011
299	05:41:44.58	-02:16:6.3	1342227049-50	083	12.800	1.000	P	20.300	2.000	11.800	1.000	P	NGC 2023-4	21 Aug 2011
300	05:41:24.21	-02:16:6.4	1342228913-14	082	1.410	1.000	P	4.150	2.000	3.260	1.000	P	NGC 2023-4	19 Sep 2011
301	05:41:44.77	-02:15:55.3	1342227049-50	083	3.070	1.000	P	nan	3.000	22.400	2.000	A	NGC 2023-4	21 Aug 2011
302	05:40:22.41	-02:15:39.7	nan		nan	0.000	A	nan	3.000	nan	0.000	A	nan	nan
303	05:42:2.62	-02:07:45.7	1342226735-36	085	1.910	1.000	A	4.140	1.000	10.700	1.000	A	NGC 2023-4	18 Aug 2011
304	05:41:45.94	-01:56:26.1	1342227047-48	086	7.530	1.000	A	nan	3.000	257.000	2.000	A	NGC 2023-4	21 Aug 2011
305	05:41:45.38	-01:51:56.8	1342227047-48	086	4.090	1.000	A	nan	3.000	nan	3.000	A	NGC 2023-4	21 Aug 2011
306	05:43:3.12	-01:48:4.6	nan		nan	0.000	A	nan	3.000	nan	0.000	A	nan	nan
307	05:41:13.85	-01:47:3.9	nan		nan	0.000	A	nan	3.000	nan	0.000	A	nan	nan
308	05:43:13.98	-01:43:10.2	nan		nan	0.000	A	0.126	1.000	nan	0.000	A	nan	nan
309	05:42:47.36	-01:24:47.0	nan		nan	0.000	A	0.193	1.000	nan	0.000	A	nan	nan
310	05:42:27.68	-01:20:1.0	1342205220-21	089	36.700	1.000	A	49.300	1.000	50.200	1.000	A	NGC 2023-4	28 Sep 2010
311	05:43:3.04	-01:16:28.9	1342228376-77	090	3.320	1.000	A	3.380	1.000	3.310	1.000	A	NGC 2023-4	9 Sep 2011
312	05:43:5.70	-01:15:54.3	1342228376-77	090	1.570	1.000	A	2.780	1.000	3.940	1.000	A	NGC 2023-4	9 Sep 2011

Table 2 continued on next page

Table 2 *(continued)*

HOPS ID	α_{J2000} h:m:s	δ_{J2000} ° :′:″	Observation Identifiers	Group Number	70μm (mJy)	flag	Method	100μm (mJy)	flag	160μm (mJy)	flag	Method	Field	Observation Date (UT)
313	05:41:0.76	-01:09:10.6	nan		nan	0.000	A	0.096	1.000	nan	0.000	A	nan	nan
314	05:46:36.12	00:20:29.2	nan		nan	0.000	A	nan	3.000	nan	0.000	A	nan	nan
315	05:46:3.63	00:14:49.2	1342205218-19	091	9.530	1.000	A	13.700	1.000	15.100	1.000	A	NGC 2068	28 Sep 2010
316	05:46:7.29	00:13:23.0	1342205218-19	091	5.730	1.000	A	nan	3.000	22.200	1.000	A	NGC 2068	28 Sep 2010
317	05:46:8.59	00:10:38.5	1342205218-19	091	6.050	1.000	A	16.400	1.000	31.500	1.000	P	NGC 2068	28 Sep 2010
318	05:46:13.50	00:08:55.3	1342205218-19	091	0.153	1.000	A	0.165	1.000	2.380	2.000	A	NGC 2068	28 Sep 2010
319	05:46:13.00	00:08:14.9	1342205218-19	091	0.027	1.000	A	nan	3.000	2.930	2.000	A	NGC 2068	28 Sep 2010
320	05:46:14.21	00:05:26.8	1342205216-17	092	0.844	1.000	P	1.700	1.000	2.500	1.000	P	NGC 2068	28 Sep 2010
321	05:46:33.17	00:00:2.2	1342215363-64	093	8.870	1.000	A	10.700	1.000	12.700	1.000	A	NGC 2068	6 Mar 2011
322	05:46:46.49	00:00:16.1	1342215363-64	093	0.816	1.000	P	4.390	2.000	32.500	2.000	A	NGC 2068	6 Mar 2011
323	05:46:47.69	00:00:25.3	1342215363-64	093	15.800	1.000	P	35.000	1.000	40.800	1.000	P	NGC 2068	6 Mar 2011
324	05:46:37.54	00:00:34.0	1342215363-64	093	3.480	1.000	A	4.820	1.000	10.700	1.000	P	NGC 2068	6 Mar 2011
325	05:46:39.25	00:01:15.0	1342215363-64	093	11.200	1.000	A	25.800	1.000	32.500	1.000	A	NGC 2068	6 Mar 2011
326	05:46:39.58	00:04:16.6	1342228365-66	094	0.805	1.000	P	nan	1.000	4.200	1.000	P	NGC 2068	9 Sep 2011
327	05:46:27.34	00:08:51.7	nan		nan	0.000	A	nan	3.000	nan	0.000	A	nan	nan
328	05:46:13.46	00:10:33.2	nan		nan	0.000	A	nan	3.000	nan	0.000	A	nan	nan
329	05:47:1.61	00:17:58.9	1342215587-88	096	6.030	1.000	P	7.820	1.000	8.810	1.000	P	NGC 2068	7 Mar 2011
330	05:46:51.37	00:19:47.4	1342218727-28	128	nan	3.000	A	nan	3.000	nan	3.000	A	NGC 2068	17 Apr 2011
331	05:46:28.32	00:19:49.4	1342228374-75	302	0.880	1.000	A	1.380	1.000	1.910	1.000	P	NGC 2068	9 Sep 2011
332	05:47:31.70	00:20:20.8	1342227966-67	303	nan	3.000	A	10.700	2.000	nan	3.000	A	NGC 2068	3 Sep 2011
333	05:47:22.88	00:20:58.3	1342227966-67	303	0.210	1.000	P	0.538	1.000	0.788	1.000	A	NGC 2068	3 Sep 2011

Table 2 continued on next page

Table 2 *(continued)*

HOPS ID	α_{J2000} h:m:s	δ_{J2000} $^{\circ}$:′:″	Observation Identifiers	Group Number	70μm (mJy)	flag	Method	100μm (mJy)	flag	160μm (mJy)	flag	Method	Field	Observation Date (UT)
334	05:46:48.53	00:21:28.2	1342218727-28	128	0.051	1.000	A	nan	3.000	1.860	2.000	A	NGC 2068	17 Apr 2011
335	05:47:5.86	00:22:38.9	1342215587-88	096	0.682	1.000	P	nan	3.000	2.780	1.000	P	NGC 2068	7 Mar 2011
336	05:46:2.28	00:23:30.7	1342216450-51	301	0.047	1.000	A	nan	3.000	0.089	1.000	A	NGC 2068	20 Mar 2011
337	05:46:55.10	00:23:34.6	1342218727-28	128	1.830	1.000	A	1.680	1.000	2.040	1.000	P	NGC 2068	17 Apr 2011
338	05:46:57.34	00:23:50.2	1342218727-28	128	0.286	1.000	P	1.300	1.000	1.730	1.000	P	NGC 2068	17 Apr 2011
339	05:45:53.59	00:25:27.3	1342216450-51	301	0.104	1.000	A	0.172	1.000	0.053	1.000	A	NGC 2068	20 Mar 2011
340	05:47:1.29	00:26:21.5	1342218727-28	128	3.120	1.000	P	15.100	2.000	10.200	1.000	P	NGC 2068	17 Apr 2011
341	05:47:0.99	00:26:22.2	1342218727-28	128	2.920	1.000	P	15.100	2.000	10.200	1.000	A	NGC 2068	17 Apr 2011
342	05:47:57.09	00:35:27.4	1342227969-70	097	0.287	1.000	A	0.339	1.000	0.717	2.000	A	NGC 2068	3 Sep 2011
343	05:47:59.03	00:35:32.9	1342227969-70	097	9.660	1.000	A	8.940	1.000	10.100	1.000	A	NGC 2068	3 Sep 2011
344	05:47:24.72	00:37:35.2	1342227971-72	098	0.086	1.000	A	0.109	1.000	0.055	1.000	A	NGC 2068	3 Sep 2011
345	05:47:38.98	00:38:36.3	1342227971-72	098	0.646	1.000	A	0.625	1.000	1.040	1.000	A	NGC 2068	3 Sep 2011
346	05:47:42.99	00:40:57.5	1342205214-15	300	0.080	1.000	A	0.071	1.000	0.219	1.000	A	NGC 2068	28 Sep 2010
347	05:47:15.89	00:21:23.8	1342215587-88	096	0.569	1.000	A	1.630	1.000	4.840	1.000	A	NGC 2068	7 Mar 2011
348	05:47:0.27	00:20:37.5	1342215587-88	096	0.682	1.000	A	nan	3.000	1.120	1.000	A	NGC 2068	7 Mar 2011
349	05:35:26.20	-05:08:33.4	1342205228-29	130	nan	3.000	A	nan	3.000	nan	3.000	A	OMC 2-3	28 Sep 2010
350	05:35:30.20	-05:08:18.9	1342205228-29	130	2.400	1.000	A	nan	3.000	23.800	2.000	A	OMC 2-3	28 Sep 2010
351	05:35:31.42	-05:04:47.1	1342205228-29	130	nan	3.000	A	nan	3.000	nan	3.000	A	OMC 2-3	28 Sep 2010
352	05:35:26.81	-05:04:3.0	1342204250-51	019	nan	3.000	A	nan	3.000	nan	3.000	A	OMC 2-3	10 Sep 2010
353	05:54:13.34	01:43:3.1	1342215365-66	000	nan	3.000	A	nan	3.000	nan	3.000	A	LDN 1622	6 Mar 2011
354	05:54:24.25	01:44:19.4	1342215365-66	000	8.430	1.000	A	37.100	1.000	37.900	1.000	A	LDN 1622	6 Mar 2011

Table 2 continued on next page

Table 2 *(continued)*

HOPS ID	α_{J2000} h:m:s	δ_{J2000} ° :′:″	Observation Identifiers	Group Number	70μm (mJy)	flag	Method	100μm (mJy)	flag	160μm (mJy)	flag	Method	Field	Observation Date (UT)
355	05:37:17.08	-06:49:49.3	1342227312-13	101	2.760	1.000	A	5.780	1.000	9.790	1.000	A	LDN 1641-N	24 Aug 2011
356	05:42:8.18	-01:26:37.5	nan		nan	0.000	A	nan	3.000	nan	0.000	A	nan	nan
357	05:41:39.10	-01:52:7.5	1342227047-48	086	6.280	1.000	A	2.900	1.000	30.200	2.000	A	NGC 2023-4	21 Aug 2011
358	05:46:7.23	00:13:29.9	1342205218-19	091	62.200	1.000	A	104.000	1.000	122.000	1.000	A	NGC 2068	28 Sep 2010
359	05:47:24.81	00:20:59.9	1342227966-67	303	20.000	1.000	A	43.600	1.000	56.100	1.000	A	NGC 2068	3 Sep 2011
360	05:47:27.09	00:20:33.1	1342227966-67	303	nan	3.000	A	6.450	1.000	nan	3.000	A	NGC 2068	3 Sep 2011
361	05:47:4.78	00:21:42.9	1342215587-88	096	1000.000	1.000	A	1080.000	1.000	1150.000	1.000	A	NGC 2068	7 Mar 2011
362	05:36:36.12	-06:38:51.9	1342227094-95	040	nan	0.000	A	nan	0.000	nan	0.000	A	LDN 1641-N	22 Aug 2011
363	05:46:43.12	00:00:52.5	1342215363-64	093	25.000	1.000	A	29.800	1.000	32.100	1.000	A	NGC 2068	6 Mar 2011
364	05:47:36.57	00:20:6.2	1342227966-67	303	85.000	1.000	A	83.900	1.000	66.500	1.000	A	NGC 2068	3 Sep 2011
365	05:47:10.62	00:21:14.1	1342215587-88	096	34.600	1.000	A	52.500	1.000	52.800	1.000	A	NGC 2068	7 Mar 2011
366	05:47:3.98	00:22:10.5	1342215587-88	096	8.230	1.000	P	27.800	2.000	97.800	2.000	A	NGC 2068	7 Mar 2011
367	05:54:36.26	01:53:54.0	1342218778-79	004	0.082	1.000	A	0.061	1.000	0.187	1.000	P	LDN 1622	18 Apr 2011
368	05:35:24.72	-05:10:30.2	1342205228-29	130	110.000	1.000	A	81.200	1.000	86.200	1.000	A	OMC 2-3	28 Sep 2010
369	05:35:26.97	-05:10:17.1	1342205228-29	130	19.600	1.000	P	nan	3.000	135.000	2.000	A	OMC 2-3	28 Sep 2010
370	05:35:27.63	-05:09:33.5	1342205228-29	130	824.000	1.000	A	702.000	1.000	597.000	1.000	A	OMC 2-3	28 Sep 2010
371	05:35:10.42	-05:55:40.9	1342204248-49	005	0.442	1.000	A	1.480	1.000	4.370	1.000	P	ONC-S	9 Sep 2010
372	05:41:26.34	-02:18:20.0	1342228913-14	082	6.460	1.000	A	16.200	1.000	29.900	1.000	A	NGC 2023-4	19 Sep 2011
373	05:46:30.68	00:02:35.3	1342215363-64	093	5.460	1.000	A	20.200	1.000	36.300	1.000	A	NGC 2068	6 Mar 2011
374	05:41:25.46	-07:55:18.9	1342205248-49	121	0.342	1.000	A	nan	3.000	11.100	2.000	A	LDN 1641-S	28 Sep 2010
375	05:39:18.36	-07:20:23.6	1342227086-87	028	0.016	1.000	A	nan	3.000	1.010	2.000	A	LDN 1641-C	22 Aug 2011

Table 2 continued on next page

Table 2 *(continued)*

HOPS ID	α_{J2000} h:m:s	δ_{J2000} $^{\circ}$:′:″	Observation Identifiers	Group Number	70μm (mJy)	flag	Method	100μm (mJy)	flag	160μm (mJy)	flag	Method	Field	Observation Date (UT)
376	05:38:18.15	-07:02:26.3	1342228171-72	033	143.000	1.000	A	117.000	1.000	77.100	1.000	A	LDN 1641-C	4 Sep 2011
377	05:38:45.54	-07:01:2.2	1342204256-57	031	6.970	1.000	P	13.400	1.000	12.800	1.000	P	LDN 1641-C	10 Sep 2010
378	05:36:25.64	-06:47:16.4	1342205238-39	038	0.882	1.000	A	0.633	1.000	4.050	2.000	A	LDN 1641-N	28 Sep 2010
379	05:37:7.71	-06:31:57.6	1342227090-91	037	0.056	1.000	A	nan	3.000	0.633	2.000	A	LDN 1641-N	22 Aug 2011
380	05:36:25.30	-06:25:2.6	1342205236-37	042	0.512	1.000	P	nan	3.000	7.660	2.000	A	LDN 1641-N	28 Sep 2010
381	05:35:7.57	-05:41:54.9	1342227098-99	013	nan	3.000	A	nan	3.000	1.630	2.000	A	ONC-S	22 Aug 2011
382	05:35:21.67	-05:37:57.9	1342205234-35	015	0.132	1.000	A	nan	3.000	0.347	1.000	A	ONC-S	28 Sep 2010
383	05:35:29.81	-04:59:51.1	1342204250-51	019	13.100	1.000	A	25.400	1.000	36.000	1.000	A	OMC 2-3	10 Sep 2010
384	05:41:44.09	-01:54:45.1	1342227047-48	086	993.000	1.000	A	914.000	1.000	987.000	1.000	A	NGC 2023-4	21 Aug 2011
385	05:46:4.77	00:14:16.3	1342205218-19	091	11.700	1.000	A	13.000	1.000	13.600	1.000	A	NGC 2068	28 Sep 2010
386	05:46:8.50	00:10:2.6	1342205218-19	091	24.500	1.000	P	54.200	1.000	45.100	1.000	P	NGC 2068	28 Sep 2010
387	05:46:7.84	00:10:0.9	1342205218-19	091	8.590	1.000	P	54.200	2.000	13.400	1.000	A	NGC 2068	28 Sep 2010
388	05:46:13.13	00:06:4.5	1342205216-17	092	32.200	1.000	A	35.100	1.000	31.200	1.000	A	NGC 2068	28 Sep 2010
389	05:46:47.02	00:00:27.0	1342215363-64	093	3.850	1.000	P	30.200	1.000	40.800	1.000	A	NGC 2068	6 Mar 2011
390	05:47:32.44	00:20:21.9	1342227966-67	303	7.700	1.000	A	10.700	1.000	14.500	1.000	A	NGC 2068	3 Sep 2011
391	05:47:17.06	00:20:53.3	1342215587-88	096	0.131	1.000	A	nan	3.000	4.390	2.000	A	NGC 2068	7 Mar 2011
392	05:46:16.48	00:21:36.0	1342228374-75	302	0.120	1.000	A	0.235	1.000	0.340	1.000	A	NGC 2068	9 Sep 2011
393	05:46:42.48	00:23:1.3	1342218727-28	128	0.146	1.000	A	nan	3.000	1.060	2.000	A	NGC 2068	17 Apr 2011
394	05:35:23.93	-05:07:53.5	1342205228-29	130	3.270	1.000	P	4.710	1.000	24.000	1.000	A	OMC 2-3	28 Sep 2010
395	05:39:17.00	-07:24:26.6	1342218729-30	026	0.100	1.000	A	0.622	1.000	2.340	1.000	A	LDN 1641-C	17 Apr 2011
396	05:39:13.15	-07:13:11.7	1342204252-53	029	0.037	1.000	A	0.263	2.000	0.219	1.000	A	LDN 1641-C	10 Sep 2010

Table 2 continued on next page

Table 2 *(continued)*

HOPS ID	α_{J2000} h:m:s	δ_{J2000} ° :′:″	Observation Identifiers	Group Number	70μm (mJy)	flag	Method	100μm (mJy)	flag	160μm (mJy)	flag	Method	Field	Observation Date (UT)
397	05:42:48.87	-08:16:10.7	1342205254-55	061	0.687	1.000	A	2.020	1.000	4.170	1.000	P	LDN 1641-S	28 Sep 2010
398	05:41:29.40	-02:21:17.1	1342228913-14	082	0.392	1.000	A	3.000	1.000	8.830	1.000	A	NGC 2023-4	19 Sep 2011
399	05:41:24.94	-02:18:8.5	1342228913-14	082	4.690	1.000	A	20.400	1.000	50.400	1.000	A	NGC 2023-4	19 Sep 2011
400	05:42:45.23	-01:16:14.2	1342228376-77	090	3.440	1.000	A	10.900	1.000	16.800	1.000	A	NGC 2023-4	9 Sep 2011
401	05:46:7.65	00:12:20.7	1342205218-19	091	0.651	1.000	A	2.540	1.000	5.170	1.000	P	NGC 2068	28 Sep 2010
402	05:46:9.97	00:12:16.8	1342205218-19	091	0.414	1.000	A	1.980	1.000	4.550	1.000	P	NGC 2068	28 Sep 2010
403	05:46:27.75	00:00:53.8	1342215363-64	093	1.580	1.000	A	5.370	1.000	12.400	1.000	A	NGC 2068	6 Mar 2011
404	05:48:7.76	00:33:50.8	1342227969-70	097	1.070	1.000	A	4.160	1.000	7.720	1.000	A	NGC 2068	3 Sep 2011
405	05:40:58.47	-08:05:36.1	1342215361-62	066	1.730	1.000	A	5.790	1.000	10.500	1.000	A	LDN 1641-S	6 Mar 2011
406	05:47:43.36	00:38:22.5	1342227971-72	098	0.469	1.000	A	1.780	1.000	3.720	1.000	P	NGC 2068	3 Sep 2011
407	05:46:28.24	00:19:27.0	1342228374-75	302	0.386	1.000	P	3.100	1.000	6.120	1.000	P	NGC 2068	9 Sep 2011
408	05:39:30.75	-07:23:59.4	1342218729-30	026	0.148	1.000	A	0.747	1.000	2.150	1.000	A	LDN 1641-C	17 Apr 2011
409	05:35:21.40	-05:13:17.5	nan		13.100	1.000	A	32.900	1.000	88.900	1.000	A	nan	nan

[a] Taken with PACS in high dynamic range mode.

[b] Taken during science demonstration phase.

REFERENCES

Adams, F., Lada, C. & Shu, F., 1987, ApJ, 312, 788

Ali, Babar, Tobin, J., J., Fischer, W. J., Poteet, C., A., Megeath, S., T., Allen, L., Hartmann, L., Calvet, N., Furlan, E. & Osorio, M., 2010, A&A, 518, L119

Konyves, V., *et al.*, 2010, A&A, 518, L106

Balog, Z., Muller, Thomas, Nielbock, Markus, Altieri, Bruno, Klass, Ulrich, Blommaert, Joris, Linz, Hendrik, Lutz, Dieter, Moor, Attila, Billot, Nicolas, Sauvage, Marc, & Okumura, Koryo, 2013, Experimental Astronomy, 38B

Cantalupo, C. M., Borrill, J. D., Jaffe, A. H., Kisner, T. S., Stompor, R. 2010 ApJS, 187, 212

Carpenter, J. M., 2000, AJ, 210, 3139

Diolaiti, Emiliano, Bendinelli, Orzio, Bonaccini, Domenico, Close, Laird, M., Currie, Douglas, G., & Parmeggiani, Gianluigi, 2000, SPIE, 4007, 879D

Dunham, M. M., Stutz, A. M., Allen, L. E., Evans, N. J., II, Fischer, W. J., Megeath, S. T., Myers, P. C., Offner, S. S. R., Poteet, C. A., Tobin, J. J. & Vorobyov, E. I.in Protostars and Planets VI, Henrik Beuther, Ralf S. Klessen, Cornelis P. Dullemond, and Thomas Henning (eds.), University of Arizona Press, Tucson, pp.195-218

Evans, Neal, J., II, *et al.*, 2009, ApJS, 181, 321

Feigelson, E. D., Getman, K., Townsley, L., Garmire, G., Preibisch, T., Groso, N., Montmerle, T., Muench, A., & McCaughrean, M. 2005, ApJS, 160, 379

Fischer, W., J., *et al.*, 2015, in prep.

Furlan, E., Fischer, W. J., Ali, B., Stutz, A. M., Stanke, T., Tobin, J. J., Megeath, S. T., Osorio, M., Hartmann, L., Calvet, N., Poteet, C.A., Booker, J., Manoj, P., Watson, D. M., & Allen, L. 2016, ApJS, 224, 5

Kennicutt, Robert, C. & Evans, Neal, J, 2012, ARA&A, 50, 531

Kryukova, E., Megeath, S., T., Hora, J., L., Gutermuth, R., A., Bontemps, S., Kraemer, K., Hennemann, M., Schneider, N., Smith, Howard, A., & Motte, F., 2014, AJ, 148, 11

McKee, C., F. & Ostriker, E., C., 2007, ARAA, 45, 565

Megeath, S. T., *et al.*, 2012, AJ, 144, 192

Lutz, D., *et al.* 2012, PACS Technical Report, PICC-ME-TN-033, http://herschel.esac.esa.int/Docs/Calibration/PACS_Point

Ott, S., 2010, ASP Conference Series, 434, 139

Piazzo, L., Ikhenaode, D., Natoli, P., Pestalozzi, M., Piacentini, F., & Traficante, A., 2012, IEEE Trans. on Image Processing, Vol. 21, Issue 8, pp. 3687-3696

Pilbratt, G.L., Riedinger, J.R., Passvogel, T., *et al.*, 2010, A&A, 518, L1

Poglitsch, A., Waelkens, C., Geis, N., *et al.*, 2010, A&A, 518, L2

Popesso, P., *et al.*, 2012, eprint arXiv:1211.4257

Reipurth, B. *et al.*, 2014 in PPVI, p 267.

Roussel, H., 2012, eprint arXiv:1205.2576

Schlafly, E. F., Green, G., Finkbeiner, D. P., Rix, H.-W., Bell, E. F., Burgett, W. S., Chambers, K. C., Draper, P. W., Hodapp, K. W., Kaiser, N., Magnier, E. A., Martin, N. F., Metcalfe, N., Price, P. A., & Tonry, J. L. 2014, ApJ, 786, 29

Stanke, T., *et al.*, 2015, in prep.

Stetson, P., B., 1987, PASP, 99, 191

Stutz, A., Launhardt, R., Linz, H., Krause, O., Henning, T., Kainulainen, J., Nielbock, M., Steinacker, J.,& Andre, P. 2010, A&A, 518, L87

Stutz, A., *et al.*, 2013, ApJ, 767, 36

Tegmark, M., 1997 ApJ, 480, 87

Tobin, J., J. 2015, ApJ, XX, YY

Werner, M. W., *et al.*, 2004, ApJS, 154, 1